Redox Biology 67 (2023) 102879

Contents lists available at ScienceDirect

Redox Biology

journal homepage: www.elsevier.com/locate/redox

Single-nucleus RNA-sequencing reveals NRF1/NFE2L1 as a key factor determining the thermogenesis and cellular heterogeneity and dynamics of brown adipose tissues in mice

Wei Shen [a,b,c,1], Suping Ren [a,b,c,1], Yongyong Hou [a,b,d,1], Zhuo Zuo [c], Shengnan Liu [a,b,c], Zhiyuan Liu [a,b,c], Jingqi Fu [a,b,c], Huihui Wang [a,b,e], Bei Yang [a,f], Rui Zhao [a,g], Yanyan Chen [h], Masayuki Yamamoto [i], Yuanyuan Xu [a,b,e], Qiang Zhang [j,**], Jingbo Pi [a,b,c,*]

[a] *Key Laboratory of Environmental Stress and Chronic Disease Control & Prevention, Ministry of Education (China Medical University), No. 77 Puhe Road, Shenyang North New Area, Shenyang, Liaoning, 110122, China*
[b] *Key Laboratory of Liaoning Province on Toxic and Biological Effects of Arsenic (China Medical University), No. 77 Puhe Road, Shenyang North New Area, Shenyang, Liaoning, 110122, PR China*
[c] *Program of Environmental Toxicology, School of Public Health, China Medical University, No. 77 Puhe Road, Shenyang North New Area, Shenyang, Liaoning, 110122, China*
[d] *Department of Nutrition and Food Hygiene, School of Public Health, China Medical University, No. 77 Puhe Road, Shenyang North New Area, Shenyang, Liaoning, 110122, China*
[e] *Group of Chronic Disease and Environmental Genomics, School of Public Health, China Medical University, No. 77 Puhe Road, Shenyang North New Area, Shenyang, Liaoning, 110122, China*
[f] *School of Basic Medical Sciences, China Medical University, No. 77 Puhe Road, Shenyang North New Area, Shenyang, Liaoning, 110122, China*
[g] *School of Forensic Medicine, China Medical University, No. 77 Puhe Road, Shenyang North New Area, Shenyang, Liaoning, 110122, China*
[h] *The First Affiliated Hospital, China Medical University, No. 155 Nanjing North Road, Heping Area, Shenyang, Liaoning, 110001, China*
[i] *Department of Medical Biochemistry, Tohoku University Graduate School of Medicine, Sendai, 980-8575, Japan*
[j] *Gangarosa Department of Environmental Health, Rollins School of Public Health, Emory University, GA, 30322, USA*

ARTICLE INFO

Keywords:
NFE2L1
brown adipocyte
BAT whitening
Lipolysis
snRNA-seq

ABSTRACT

Brown adipose tissue (BAT) is a major site of non-shivering thermogenesis in mammals and plays an important role in energy homeostasis. Nuclear factor-erythroid 2-related factor 1 (NFE2L1, also known as Nrf1), a master regulator of cellular metabolic homeostasis and numerous stress responses, has been found to function as a critical driver in BAT thermogenic adaption to cold or obesity by providing proteometabolic quality control. Our recent studies using adipocyte-specific *Nfe2l1* knockout [*Nfe2l1*(f)-KO] mice demonstrated that NFE2L1-dependent transcription of lipolytic genes is crucial for white adipose tissue (WAT) homeostasis and plasticity. In the present study, we found that *Nfe2l1*(f)-KO mice develop an age-dependent whitening and shrinking of BAT, with signatures of down-regulation of proteasome, impaired mitochondrial function, reduced thermogenesis, pro-inflammation, and elevated regulatory cell death (RCD). Mechanistic studies revealed that deficiency of *Nfe2l1* in brown adipocytes (BAC) primarily results in down-regulation of lipolytic genes, which decelerates lipolysis, making BAC unable to fuel thermogenesis. These changes lead to BAC hypertrophy, inflammation-associated RCD, and consequently cold intolerance. Single-nucleus RNA-sequencing of BAT reveals that deficiency of *Nfe2l1* induces significant transcriptomic changes leading to aberrant expression of a variety of genes involved in lipid metabolism, proteasome, mitochondrial stress, inflammatory responses, and inflammation-related RCD in distinct subpopulations of BAC. Taken together, our study demonstrated that NFE2L1 serves as a vital transcriptional regulator that controls the lipid metabolic homeostasis in BAC, which in turn determines the metabolic dynamics, cellular heterogeneity and subsequently cell fates in BAT.

* Corresponding author. Key Laboratory of Environmental Stress and Chronic Disease Control & Prevention, Ministry of Education (China Medical University), No. 77 Puhe Road, Shenyang North New Area, Shenyang, Liaoning, 110122, China.
** Corresponding author.
E-mail addresses: qiang.zhang@emory.edu (Q. Zhang), jbpi@cmu.edu.cn, jingbopi@163.com (J. Pi).
[1] These authors contributed equally to this work.

https://doi.org/10.1016/j.redox.2023.102879
Received 3 August 2023; Received in revised form 30 August 2023; Accepted 5 September 2023
Available online 11 September 2023

1. Introduction

Abbreviations:

Adgre1	adhesion G protein-coupled receptor E1
Adipoq	adiponectin
ANOVA	analysis of variance
APP	antigen processing and presentation
AT	adipose tissues
Atgl/Pnpla2	adipocyte triglyceride lipase/patatin-like phospholipase domain containing 2
BAC	brown adipocyte
BAT	brown adipose tissue
Casp1	caspase 1
CNC-bZIP	cap 'n' collar-basic leucine zipper protein
CO_2	carbon dioxide
COX	cytochrome *c* oxidase
Cpt1b	carnitine palmitoyltransferase 1 B
DEGs	differentially expressed genes
Elovl	ELOVL fatty acid elongase
ER	endoplasmic reticulum
FFAs	free fatty acids
Fis1	mitochondrial fission protein 1
GPR3	G protein-coupled receptor 3
GSEA	gene set enrichment analysis
gWAT	gonadal WAT
H&E	hematoxylin and eosin
Hsl	hormone-sensitive lipase
IHC	immunohistochemistry
Ifng	interferon γ
Il1b	interleukin 1β
iWAT	inguinal WAT
KEGG	Kyoto encyclopedia of genes and genomes
LDs	lipid droplets
MAC	macrophages
Mgl	monoacylglycerol lipase
NC	nerve cells
NK/T	natural killer/T cells
Ndufs4	NADH dehydrogenase (ubiquinone) Fe–S protein 4
NFE2L1/NRF1	nuclear factor erythroid 2-related factor 1
Nfe2l1(f)-KO	adipocyte-specific Nfe2l1 knockout
Nlrp3	NLR family pyrin domain containing 3
NST	non-shivering thermogenesis
OCR	oxygen consumption rate
Opa1	optic atrophy 1 mitochondrial dynamin like GTPase
ORO	oil red-O
OXPHOS	oxidative phosphorylation
Pgc-1α	peroxisome proliferator-activated receptor gamma coactivator-1 α
PKA	protein kinase A
Plin1	perilipin 1
PPAR	peroxisome proliferator-activated receptor
Prdm16	PR domain containing 16
Pycard	apoptosis-associated speck-like protein containing a CARD
RCD	regulatory cell death
RT-qPCR	reverse transcription-quantitative polymerase chain reaction
snRNA-seq	single-nucleus RNA sequencing
SNP	single nucleotide polymorphism
TAG	triacylglycerol/triglyceride
TEM	transmission electron microscopy
Ucp1	uncoupling protein 1
VEC	vascular endothelial cells
WAT	white adipose tissue
WAC	white adipocyte

The epidemic outburst of obesity and related metabolic disorders has directed research attention to the physiology of distinct adipocytes and fat depots. The adipose tissue (AT) is not only a depot for storing excessive energy but also a crucial metabolic sensor and endocrine organ coordinating a wide range of physiological processes [1–3]. In contrast to white adipocytes (WAC), which store energy as triglycerides (TAG) in unilocular lipid droplets, brown adipocytes (BAC) have highly enriched mitochondria and multilocular lipid droplets. BAC utilizes free fatty acids (FFAs) and glucose at a high rate mainly mediated by uncoupling protein 1 (UCP1) which uncouples the energy of mitochondrial proton gradient from ATP synthesis, dissipating the energy instead in the form of heat. BAC thermogenesis, also referred to as non-shivering thermogenesis (NST), is a dynamic and precisely controlled process, the failure of which may bring devastating consequences to the body [4]. Thus, the function and plasticity of BAT are crucial for the human body to adapt to environmental cues. Dysfunctional BAT is implicated in the pathogenesis of various metabolic disorders, including obesity and diabetes [5]. While BAT has long been recognized as a highly homogeneous population of BAC, cellular heterogeneity of BAT was recently revealed by single-cell/nucleus RNA-sequencing (sc/nRNA-seq) technique showing that distinct subpopulations of BAC exist in the tissue [6,7].

The cap 'n' collar-basic leucine zipper protein (CNC-bZIP) nuclear factor erythroid 2-related factor 1 (NFE2L1, also known as NRF1) is a master regulator controlling the transcription of a suite of genes involved in proteasomal homeostasis, cell metabolism and numerous stress responses, antioxidant response in particular [8–11]. A single nucleotide polymorphism (SNP), rs3764400, in the 5′-flanking region of the human *NFE2L1* gene, appears to be associated with obesity in humans [12–15]. In addition, an epigenome-wide association study identified human *NFE2L1* as one of the genes nearest to the sentinel methylation markers of a locus linked to BMI and adverse outcomes of obesity [15,16]. In line with the findings that NFE2L1 is potentially involved in the pathogenesis of obesity, BAC-specific deletion of *Nfe2l1* in mice resulted in endoplasmic reticulum (ER) stress, tissue inflammation, markedly diminished mitochondrial function and whitening of the BAT, highlighting NFE2L1 as a critical driver in proteasomal adaption under thermogenic conditions [9,17]. Our recent studies demonstrated that adipocyte-specific *Nfe2l1* knockout [*Nfe2l1*(f)-KO] mice, in which the *Nfe2l1* gene was disrupted specifically in the adiponectin-expressing adipocytes, exhibit a dramatically reduced subcutaneous adipose tissue mass, adipocyte hypertrophy, and severe adipose inflammation mediated via disturbed expression of lipolytic genes in adipocytes [18–20]. In addition, NFE2L1 regulates adipogenesis in an isoform-specific manner. Specifically, the long isoforms of NFE2L1 negatively regulate the transcription of peroxisome proliferator-activated receptor γ (*Pparγ*), *Pparγ2* in particular, and thereby suppress adipogenesis [21]. Given that NFE2L1 controls WAC plasticity by regulating the transcription of multiple lipolytic genes and *Pparγ*, which are also crucial to the function and homeostasis of BAC, we speculate that *Nfe2l1* deficiency may cause downregulation of lipolytic genes and induction of *Pparγ* in BAC, and thus results in lipid overload leading to inflammatory response and other consequences in BAT. Although the crucial roles of NFE2L1 in adipocyte biology have been investigated by using two distinct lines of mouse models with BAC or

mature adipocyte-specific knockout of *Nfe2l1,* the effect of *Nfe2l1* loss on the cellular heterogeneity and metabolic dynamics of BAT, BAC subpopulations in particular, has not been investigated at the single-cell level. Such studies would be helpful to understand the molecular mechanisms of adaptive NST response and cellular dynamics of BAT.

In the present study, we found that deletion of *Nfe2l1,* mediated by adiponectin promoter-driven Cre recombinase in mice, induces an age-dependent whitening and shrinking of BAT and cold intolerance. The mRNA profiles of BAT showed signatures of down-regulated proteasome subunits, mitochondrial dysfunction, pro-inflammatory response, and augmented inflammation-related regulatory cell death (RCD). Mechanistic studies revealed that deficiency of *Nfe2l1* in BAC primarily decreases the expression of multiple lipolytic genes and thus disturbs lipid metabolism leading to BAC hypertrophy and inflammatory responses in BAT. snRNA-seq analysis of BAT reveals that NFE2L1 is a key factor determining the cellular heterogeneity and dynamics and thus homeostasis of BAC.

2. Materials and methods

2.1. Animals and treatments

Nfe2l1(f)-KO mice were produced by crossing the mice carrying *Nfe2l1*^{flox} allele [22] and Cre recombinase gene driven by the promoter of *adiponectin* gene (*Adipoq*-Cre, 010,803, Jackson Labs Technologies, Inc., Sacramento, CA) as described previously [18]. *Nfe2l1*(f)-KO mice carrying the genotype of *Nfe2l1*$^{flox/flox}$;*Adipoq*-Cre^{+} and their littermates with the genotype of *Nfe2l1*$^{flox/flox}$;*Adipoq*-Cre^{-} (Flox) were used in the current study. Genotyping was performed using PCR on genomic DNA isolated from tail snips. The sequence of genotyping primers is given in Supplementary Table S1. Mice were housed on a 12 h/12 h light/dark cycle, 24 °C and 50% humidity. Mice were given distilled water and a standard laboratory chow diet (Cat# SWS9102, Jiangsu Xietong Organism Co, Ltd, Nanjing, China) *ad libtum* unless otherwise specified. For acute cold exposure, mice fasted for 12 h were placed in a cage maintained at 4 ± 1 °C for 4 h. For chronic cold adaptation (8 °C for 14 days), mice were housed in cages with *ad libitum* access to a chow diet and water with a 12 h light/dark cycle. In the intervention studies, mice were administered with CL316243 (1 mg/kg/d, C5976, Sigma) by intraperitoneal injection for 7 days, followed by metabolic measurements and tissue collection. Mice were euthanized and various relevant tissues were collected and weighed after relevant treatments. Tissue samples were stored at –80 °C until subsequent determination. Group size was 7–8 mice per group. All animal procedures followed the ARRIVE guidelines and were approved by the Animal Ethics Committee of China Medical University (#1408 M).

2.2. Measurements of core temperature and energy metabolism in mice

Rectal body core temperature was measured using a probe attached to a digital thermometer (BAT-10 thermometer, Physitemp, Clifton, NJ, USA). An 8-channel PromethION etabolic system (Sable Systems International, Las Vegas, Nevada, USA) was used to monitor energy expenditure and respiration in mice. Mice were housed at 24 °C or 4 °C in the PromethION metabolic cages (1 mouse per cage) placed in a temperature-controlled cabinet. The basic metabolic indicators, including diet consumption, O_2 consumption and CO_2 production, were monitored in real-time according to the manufacturer's instructions.

2.3. Histological examination

The interscapular BAT sections were stained with hematoxylin and eosin (H&E) and immunohistochemistry (IHC) as described previously [18,19]. In brief, BAT was dissected and subjected to fixation in 4% paraformaldehyde for at least 24 h. Then, tissues were dehydrated step by step with ethanol and embedded in paraffin. As the liquid paraffin solidified, serial sections (4 μm) were obtained via the HistoCore AUTOCUT R-Automated Rotary Microtome (Leica, Nussloch, Germany) followed by H&E staining. For IHC staining, the primary antibody against F4/80 (sc-25830, Santa Cruz Biotechnology Inc., CA, USA) was used and followed by DAB staining (ZLI-9019, Zhongshan Golden Bridge BioTech, Co., Ltd., Beijing, China). Regarding oil red-O (ORO) staining, the BAT flash-frozen with liquid N_2 immediately after collection were embedded in O·C.T compound and sectioned into 10-μm-thick slices. ORO stain (0.3% w/v ORO in 60% v/v isopropanol) was added and incubated for 40 min at room temperature [23]. Imaging of pathological changes was performed using an optical microscope (200*x*, DMi8, Leica).

2.4. Transmission electron microscopy (TEM)

Tissue pieces (2 mm × 2 mm × 2 mm) isolated from the centric part of interscapular BAT were fixed in 2.5% glutaraldehyde-0.1 M cacodylate buffer at 4 °C for 4 h at least, followed by washing with 0.1 M cacodylate buffer for 15 min twice. Then the samples were further fixed with 1% (w/v) osmium tetroxide (OsO_4) at 4 °C for 2 h, cleared in 0.1 M cacodylate buffer twice, and serially dehydrated with 50, 70, 80, 90, and 95% acetone for 15 min each followed by 3 times of 100% acetone dehydration. The resulting specimens were preserved in a mixture of epoxy resins and acrylic overnight, then embedded with beam capsules filled with 100% resin and aggregated at 60 °C for 48 h. Sections (60 nm) prepared using an ultramicrotome (Leica EM UC6, Germany) were examined by TEM (JEM-1400 Flash, Japan) and photographed at different magnifications ranging from 2000 to 20,000 × .

2.5. Bulk RNA-sequencing and data analysis

RNA isolation, purification, quality control, and sequencing library preparation and data pre-analysis were conducted as detailed in Supplementary Materials and Methods, Section 2.5. Genes differentially expressed between groups were identified using the DESeq2 package (version 1.36.0). A p-value cutoff of 0.05 and fold-change cutoff of 2 were used for statistical significance of gene expression changes. Gene set enrichment analysis (GSEA) was completed using clusterProfiler package (version 4.4.1), using pathways from Kyoto Encyclopedia of Genes and Genomes (KEGG) database.

2.6. RNA isolation and RT-qPCR

RNA isolation and RT-qPCR were performed as described previously [24]. Briefly, according to manufacturer's instructions, total RNA of BAT was extracted using TissueLyser II with TRIzol (#15596, Invitrogen Corporation, Carlsbad, CA, USA), subsequently precipitated with isopropanol and subjected to clean-up using 75% ethanol. RNA concentrations were measured using the NanoDrop 2000c Spectrophotometer (Thermo Fisher Scientific Inc., Waltham, MA, USA). Reverse transcription was conducted using a commercial kit (#RR037A, Takara Biomedical Technology, Co., Ltd., Dalian, China). SYBR Premix Ex Taq (#RR420A, Takara Biomedical Technology, Co., Ltd., Dalian, China) was used for qPCR. Amplification of cDNA and fluorescence measurement was performed using an ABI Q6 Flex Real-time PCR System (Applied Biosystems Inc., Foster City, CA). Each tissue sample was measured in triplicate and resulting average was used for further statistical analysis. Primers were designed using Primer Express 4 and Primer Blast (http://www.ncbi.nlm.nih.gov/tools/primer-blast/) software and synthesized by Life Technologies (Shanghai, China). The sequences are shown in Table S2. The expression level of *36B4* was used as the loading control and the relative expression of genes is shown as fold-change over control (2-ΔΔCt).

2.7. Protein extraction and western blotting

Water soluble proteins were isolated by pulverizing frozen adipose tissues in a lysis buffer purchased from Cell Signaling Technology Inc. (#9803, Danvers, MA, USA) containing both proteinase and phosphatase inhibitors (P8340, P5726 and P0044, Sigma). Protein concentrations were determined using a BCA assay kit (#P0010, Beyotime Biotechnology, Suzhou, China). Immunoblot analysis was performed as previously described [20]. Equal amounts of protein were resolved using SDS-PAGE gels. The following antibodies were used for detecting specific proteins: UCP1 (#ab23841, 1:1000), PGC-1α (#ab54481, 1:1000), OXPHOS (#ab110413, 1:1000), FIS1 (#ab71498, 1:1000) and OPA1 (#ab42364, 1:1000) were purchased from Abcam Inc. (Cambridge, MA, USA); COX IV (#4844, 1:1000), PLIN1 (#9349, 1:1000) and ATGL (2138, 1:1000) were from Cell Signaling Technology; NDUFS4 (O43181, 1:1000) was from Thermo Fisher Scientific; HSL (sc-25843, 1:1000), MGL (sc-398,942, 1:1000) and β-ACTIN (sc-47778, 1:3000) were obtained from Santa Cruz Biotechnology. Quantification of immunoreactive bands was carried out with the Image J software (National Institutes of Health, USA).

2.8. Assay of lipolytic activity

BAT minced at around 2 mm in diameter were incubated with a glycerol-free basic medium containing 10 μM CL316243 (C5976, Sigma). Following a 2-h incubation at 37 °C and 5% CO_2, the resulting media were collected and applied to determine the content of glycerol with a commercial kit (K622, BioVision Inc., Milpitas, CA). Glycerol release was calculated according to the instructions and normalized by tissue weight or protein content.

2.9. snRNA-seq

The mixed BAT samples from 3 mice of each genotype (4 weeks old, female) were rinsed with pre-cooled RNase-free saline, cut into small pieces on ice and stored at −80 °C. Nuclear suspensions were loaded on a 10x Genomics GemCode Single-cell instrument that generates single-cell Gel Bead-In-EMlusion (GEMs). Libraries were generated and sequenced from the cDNAs with Chromium Next GEM Single Cell 3′ Reagent Kits v3.1. Silane magnetic beads were used to remove leftover biochemical reagents and primers from the post-GEM reaction mixture. Full-length, barcoded cDNAs were then amplified by PCR to generate sufficient mass for library construction. R1 (read 1 primer sequence) was added to the molecules during GEM incubation. P5 and P7, the sample indexes, and R2 (read 2 primer sequence) were added during library construction via End Repair, Atailing, Adaptor Ligation, and PCR. The final libraries contained the P5 and P7 primers used in Illumina bridge amplification. The Single Cell 3′ Protocol produced Illumina-ready sequencing libraries. A Single Cell 3′ Library comprised standard Illumina paired-end constructs which begin and end with P5 and P7. The Single Cell 3' 16 bp 10x Barcode and 10 bp UMI were encoded in Read 1, while Read 2 was used to sequence the cDNA fragment. Sample index sequences were incorporated as the i7 index read. Read 1 and Read 2 were standard Illumina® sequencing primer sites used in paired-end sequencing.

2.10. snRNA-seq data analysis

The count matrix generation, filtering, normalization, clustering and *t*-SNE generation were conducted as detailed in Supplementary Materials and Methods, Section 2.10. The enrichment analysis, gene set score, and trajectory analysis were performed as follows.

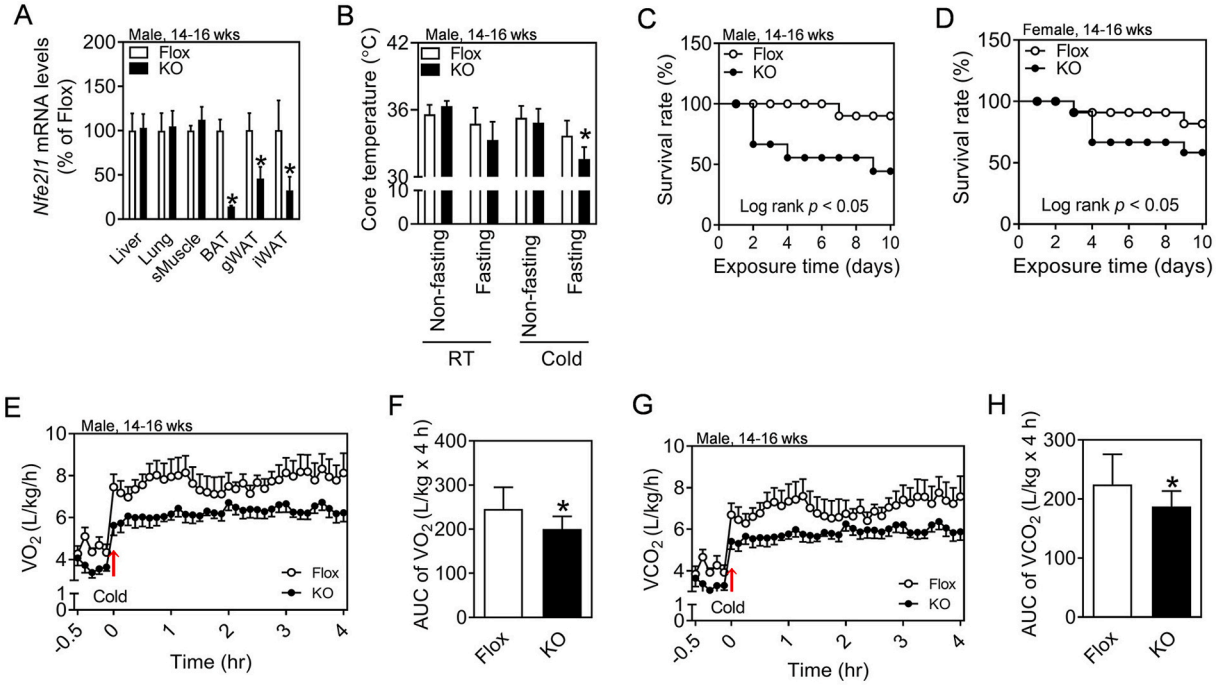

Fig. 1. The core temperature, survival rate and energy expenditure of *Nfe2l1*(f)-KO mice under cold challenge. (A) mRNA levels of *Nfe2l1* in the tissues of *Nfe2l1*(f)-KO (KO) mice relative to their *Nfe2l1*$^{flox/flox}$ (Flox) littermates. sMuscle, skeletal muscle; BAT, interscapular brown adipose tissue; gWAT, gonadal white adipose tissue; iWAT, inguinal white adipose tissue. N = 6–8. *$p < 0.05$ vs the same tissue of Flox mice. (B) The rectal temperature of mice under room tempreture (RT, 24 °C) or following acclimation to cold for 4 h (Cold, 4 °C). The mice were either fasted for 16 h overnight or given *ad libtum* access to chow diet before the cold exposure. N = 6–8. *$p < 0.05$ vs Flox. (C and D) The survival rates of male and female mice under sustained cold exposure (8 °C). N = 6–8. *$p < 0.05$ vs Flox. (E and G) The oxygen consumption rate (E) and CO_2 production rate (G) of male mice in response to acute cold exposure. VO_2, volume of O_2 consumed; VCO_2, volume of CO_2 produced. N = 8. (F and H) The quantitative areas under curves (AUC) of (E) and (G), respectively. *$p < 0.05$ vs Flox. (For interpretation of the references to color in this figure legend, the reader is referred to the Web version of this article.)

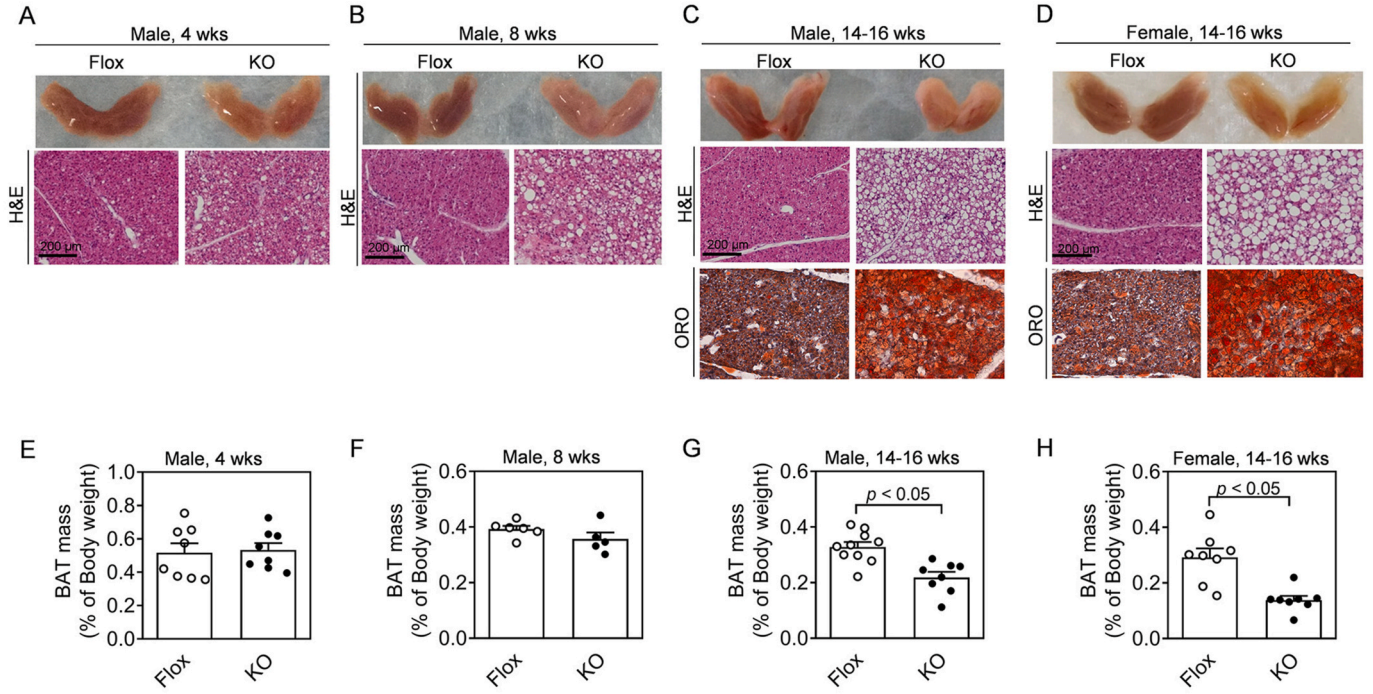

Fig. 2. The morphology and mass of BAT in *Nfe2l1*(f)-KO mice at different ages. (A–C) Representative images of gross (upper), H&E stained (middle), and ORO stained (lower) of BAT in male *Nfe2l1*(f)-KO (KO) and Flox control mice at ages of 4 (A), 8 (B) and 14–16 (C) weeks, respectively. Scale bar, 200 μm. (D) Representative images of gross (upper), H&E stained (middle), and ORO stained (lower) of BAT of female *Nfe2l1*(f)-KO (KO) and Flox mice at age of 14–16 weeks. (*E*–G) The ratio of BAT weight to body weight of male mice at age of 4, 8, and 14–16 weeks, respectively. (H) The ratio of BAT weight to body weight of female mice at age of 14–16 weeks. N = 6. *$p < 0.05$ vs Flox.

2.10.1. Enrichment analysis

The differentially expressed genes (DEGs) were further divided into up- and down-regulated groups for **KEGG** pathway enrichment analysis by using clusterProfiler package and pathways with FDR <0.05 were shown.

2.10.2. Gene set score

Gene set scores were calculated using the Seurat function AddModuleScore which calculates the average expression of a given signature per cell and subtracts it from the average expression of randomly selected control features. AddModuleScore was run using 500 control features. The proteasome gene set was formed by *Psmd1, Psmd11, Psmd14, Psmc6, Psmd12, Psma1, Psmd3,* and *Psmd4*. This list contains genes from the mmu 03050 of KEGG "Proteasome'' that were downregulated in the combination of A0, A1, A2 subclusters in *Nfe2l1*(f)-KO (KO) compared to *Nfe2l1*$^{flox/flox}$ (Flox). The AMPK gene set was formed by *Pparg, Igf1r, Ppp2r3a, Eef2k, Camkk2,* and *Prkag2*, containing genes from the mmu 04152 of KEGG "AMPK signaling pathway'' that were downregulated in the combination of A0, A1, A2 subclusters in KO. The APP gene set was formed by *Tap1, Tap2, H2-T22, Tapbp, H2-T23, Psme1, Ctsb, B2m, H2–K1* and necroptosis gene set was formed by *Stat1, Stat2, Mlkl, Stat3, Glul, Eif2ak2, Bid, Irf9, Ifngr1, Camk2d,* and *Fas*. These two gene sets are from the mmu 04612 and mmu 04217 of KEGG and they are upregulated in A3 of Flox compared to the combination of A0, A1, and A2 subclusters in Flox. Statistical analysis was performed by a two-sided Wilcoxon rank sum test followed by BH correction.

2.10.3. Trajectory analysis

RNA velocity analysis was conducted by using scVelo v.0.2.3. In particular, to count spliced and unspliced reads for each sample, the 10 × velocyto pipeline was run in the filtered cell ranger-generated BAM files, while for single-nucleus RNA velocity inference, the dynamical model of scVelo was applied [25].

2.11. Statistics

All statistical analyses of non-omics data were performed using GraphPad Prism 8 (GraphPad Software, San Diego, CA), with $p < 0.05$ considered as significant. Data were expressed as mean ± standard deviation (SD). For comparisons between the two groups, a two-tailed unpaired Student's *t*-test was performed. When the difference among three or more groups was evaluated, one-way analysis of variance (ANOVA) or, when appropriate, two-way ANOVA followed by Bonferroni's test was used. Statistical analyses of omics data were all performed in R, and details of the packages used and statistical test methods can be viewed in the corresponding sections.

2.12. Data and code availability

Our snRNA-seq and bulk RNA-seq data have been deposited in NCBI Gene Expression Omnibus (GEO) database (accession number: GSE225281). The dataset of low- and high-thermogenic adipocytes can be downloaded from GEO databases with accession number of GSM3567479. The dataset of adipocytes that regulates thermogenesis can be accessed from public database ArrayExpress with accession number E-MTAB-8562. All the code for analysis and plotting in R is available on GitHub (https://github.com/SEVEN1003/BAT).

3. Results

3.1. Thermogenesis is impaired in adult Nfe2l1(f)-KO mice

To verify the efficiency and specificity of *Adipoq*-Cre mediated *Nfe2l1* knockout, we first analyzed the mRNA levels of *Nfe2l1* in different tissues of *Nfe2l1*(f)-KO mice. As shown in Fig. 1A, the mRNA levels of *Nfe2l1* were significantly decreased in interscapular BAT, gonadal WAT (gWAT) and inguinal WAT (iWAT) of *Nfe2l1*(f)-KO mice, but not in the tissues with low *Adipoq* expression, including liver, lung and skeletal

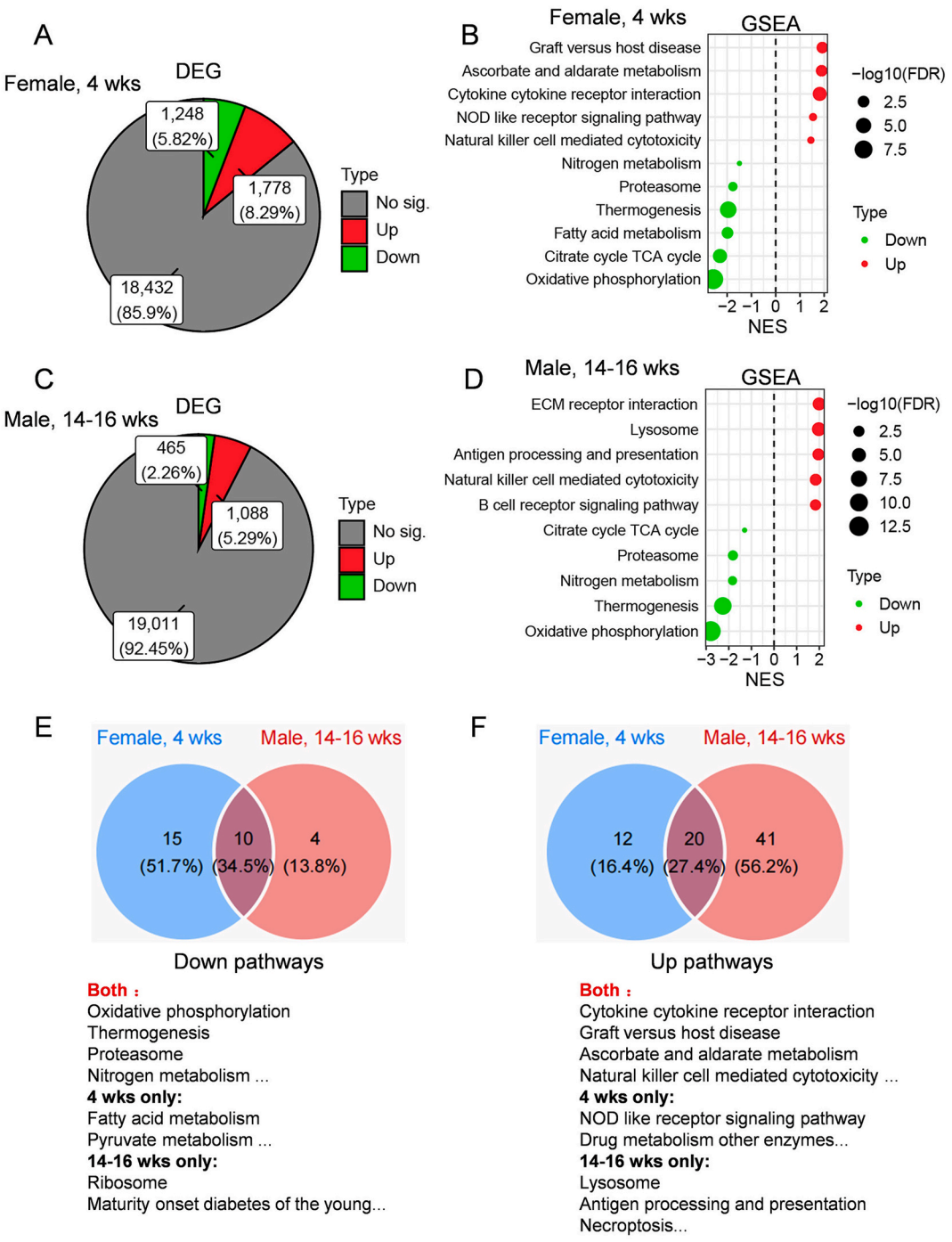

Fig. 3. Analysis of bulk RNA-seq data of BAT of 4 weeks old female and 14–16 weeks old male *Nfe2l1*(f)-KO mice. (A–D) Pie charts of DEGs (A and C) and bubble charts of gene set enrichment analysis (GSEA) (B and D) of female mice at 4 weeks of age (A and B, n = 3) and male mice at 14–16 weeks of age (C and D, n = 3). The first 5–6 pathways that were significantly up- or down-regulated and closely related to BAT function or phenotype are displayed, with direction of changes indicated by color and significance level indicated by dot size. The X and Y axes represent normalized enrichment score (NES) and term name, respectively. (E and F) Venn diagrams of the pathways down-regulated (E) or up-regulated (F) in GSEA. (For interpretation of the references to color in this figure legend, the reader is referred to the Web version of this article.)

muscle. In addition, the protein levels of NFE2L1 in BAT were analyzed by western blotting. As illustrated in Supplementary Fig. S1, multiple protein bands around 95–110, 85, 65, and 42–45 kDa decreased substantially in the KO mice compared to their littermate controls. To investigate whether the loss of *Nfe2l1* in adipocytes affects the thermogenic function of adipose tissues, we analyzed the core temperature of adult *Nfe2l1*(f)-KO mice under different conditions. While the rectal temperature of mice at room temperature showed no significant differences between genotypes with or without fasting, 4 h cold exposure induced a significant reduction in the core body temperature in fasting *Nfe2l1*(f)-KO mice, but not in Flox controls with the same temperature treatments (Fig. 1B). In agreement with findings with acute cold exposure, the survival rates of male (Fig. 1C) and female (Fig. 1D) *Nfe2l1*(f)-KO mice following sustained cold exposure for up to 10 days were much lower than those in Flox mice. To ascertain the impaired adaptive thermogenesis in *Nfe2l1*(f)-KO mice, we monitored O_2

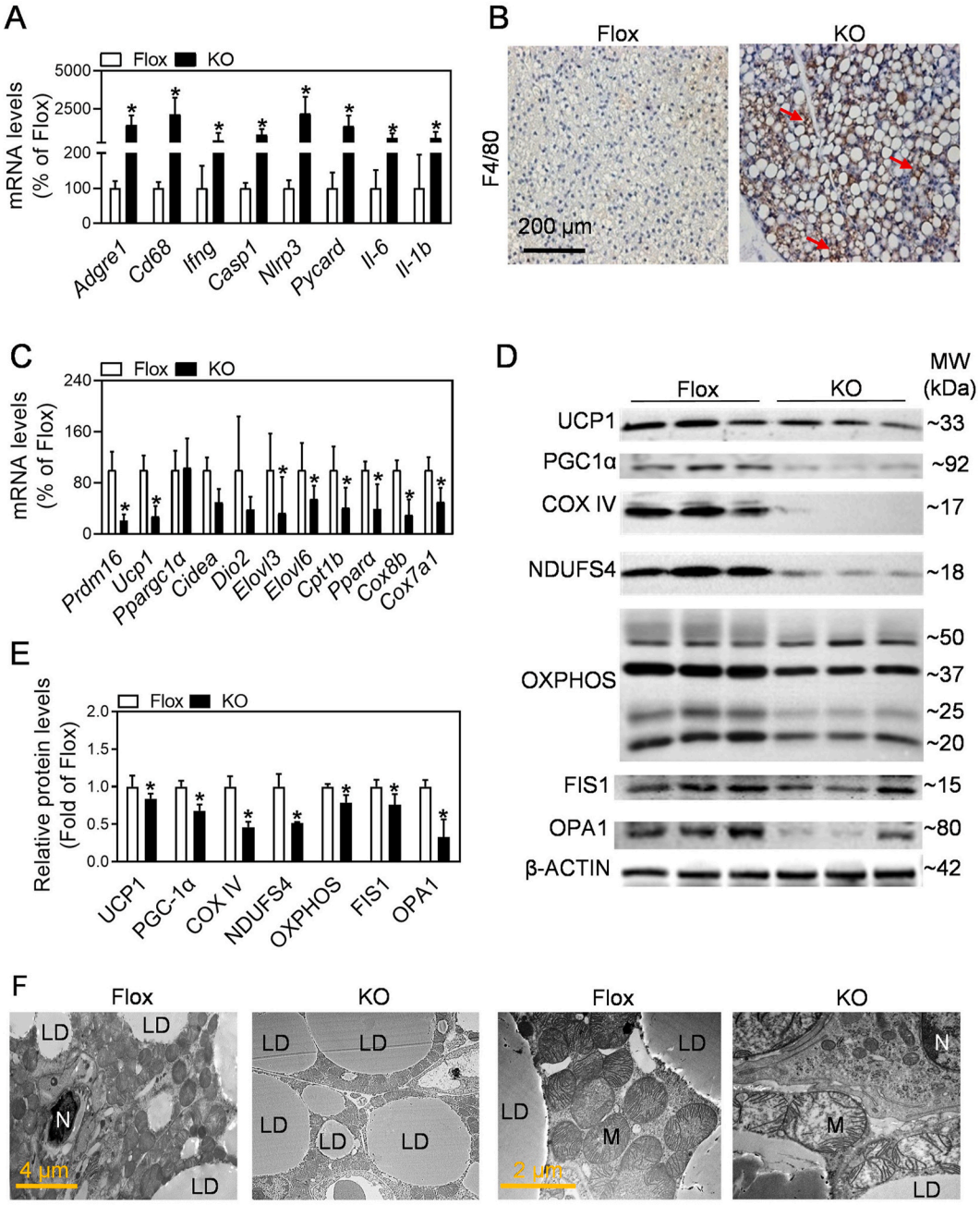

Fig. 4. The mRNA and protein expression profiles and electron microscopy of the BAT of adult male *Nfe2l1*(f)-KO mice at age of 14–16 weeks. (A and C) Relative mRNA expression of genes related to inflammatory cell death (A) and thermogenic function (C). N = 7–8. *$p < 0.05$ vs Flox. (B) Representative histological images (20 ×) of IHC for F4/80 of BAT. Bar, 200 μm. Red arrows, hypertrophic adipocytes surrounded by F4/80-positive macrophages. N = 3. (D) Representative immunoblot for protein expression of genes involved in BAT function. (E) Densitometry analyses of Western blotting. N = 6–8. *$p < 0.05$ vs Flox. (F) Representative electron microscopy images of BAT. n = 3. LD, lipid droplets; M, mitochondria; N, Nuclei. (For interpretation of the references to color in this figure legend, the reader is referred to the Web version of this article.)

consumption and CO_2 production using metabolic cages. At conventional rearing temperatures (24 °C), the O_2 consumption and CO_2 production of *Nfe2l1*(f)-KO mice were slightly lower than those of Floxed mice, especially at night (Supplementary Fig. S2). After the mice were challenged with cold (4 °C), *Nfe2l1*(f)-KO mice displayed a substantially subdued increase of O_2 consumption and CO_2 production compared to Flox mice (Fig. 1E–H).

3.2. *Nfe2l1(f)-KO mice display an age-dependent whitening and shrinking of BAT*

To understand the cellular mechanisms underlying cold intolerance in *Nfe2l1*(f)-KO mice, we first examined the mass and morphological changes of BAT. As shown in Fig. 2, *Nfe2l1*(f)-KO mice show whitening and shrinking of interscapular BAT in an age-dependent manner. Specifically, morphological and histological analysis revealed that the BAT of male Flox mice showed a certain degree of whitening with increasing age, whereas *Nfe2l1*(f)-KO mice at the same age of week had more lipid accumulation in BAT, characterized by large monocellular lipid droplets (Fig. 2A–C). In agreement with the phenotype of male mice, female *Nfe2l1*(f)-KO mice at 14–16 weeks old showed evident BAT whitening (Fig. 2D). Although there were no significant differences in BAT mass between the two genotypes at 4 and 8 weeks of age (Fig. 2E and F), dramatic reductions of BAT mass in *Nfe2l1*(f)-KO mice at 14–16 weeks of

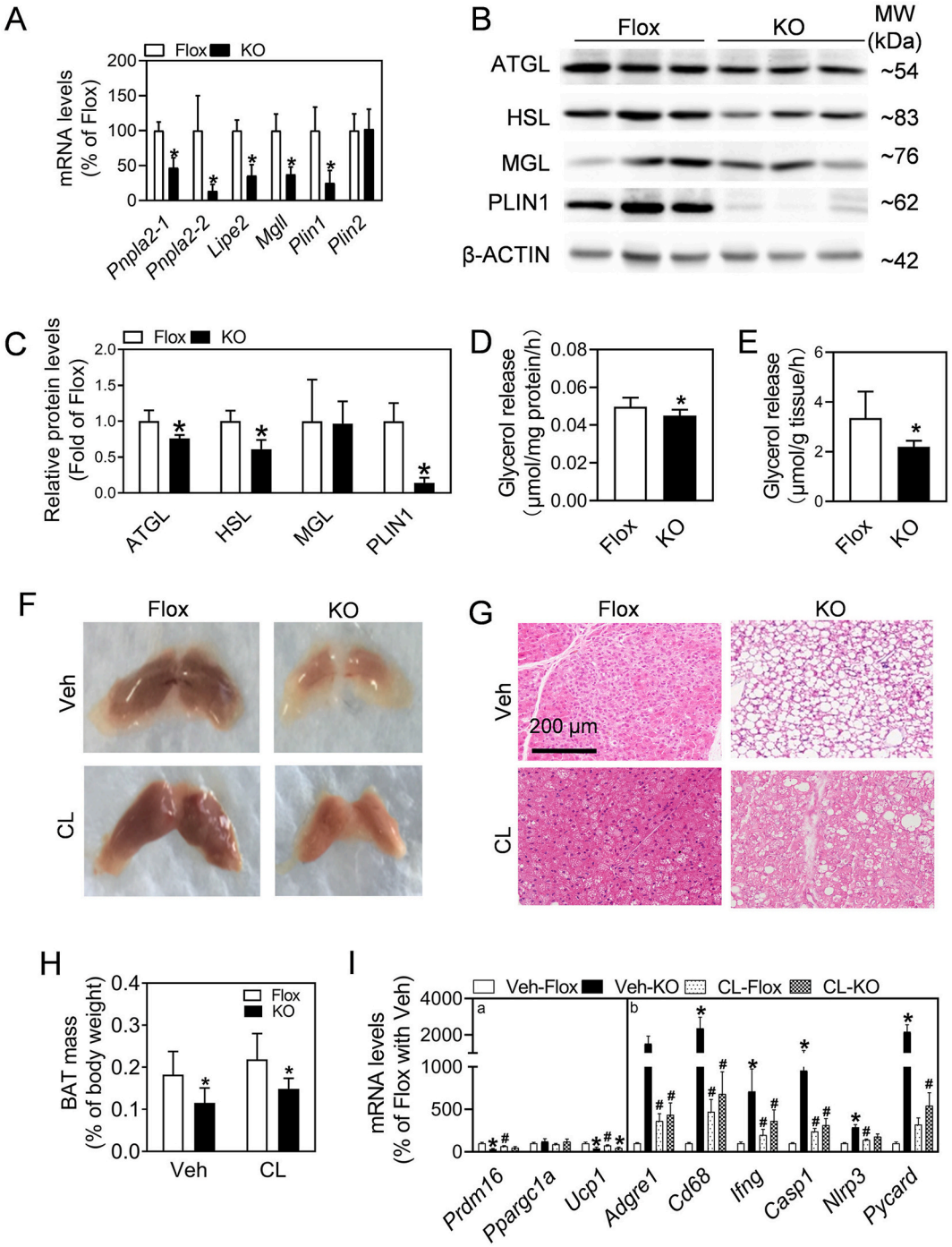

Fig. 5. Activation of lipolytic enzymes via a post-translational mechanism by CL316243 treatment reverses partially the severe inflammatory response in the BAT of *Nfe2l1*(f)-KO mice. (A) The mRNA expression of major lipolytic genes in the BAT of adult male *Nfe2l1*(f)-KO mice at age of 14–16 weeks. N = 7–8. *$p <$ 0.05 vs Flox. (B) Representative images of immunoblotting of lipolytic proteins. (C) Densitometry analyses of proteins in (B). N = 3, *$p < 0.05$ vs Flox. (D and E) Lipolytic activity of BAT under basal (D) and CL316243-stimulated condition *in vitro* (E). N = 3. *$p < 0.05$ vs Flox. (F and G) Representative images of gross (F) and H&E stained (G) BAT from 5-week-old male *Nfe2l1*(f)-KO and Flox mice that had been treated with CL316243 for 7 days. (H) The ratio of BAT to body weight of mice under the same conditions as (F and G). (I) Normalized thermogenic (a) and inflammation (b) gene expression in BAT from mice treated as in (F–H). N = 7–8. Veh-Flox, Flox treated with Veh; Veh-KO, *Nfe2l1*(f)-KO mice treated with Veh; CL-Flox, Flox treated with CL316243; CL-KO, *Nfe2l1*(f)-KO mice treated with CL316243. #$p < 0.05$ vs Veh of the same genotype; *$p < 0.05$ vs Flox with the same treatment.

age under chow diet were observed in both genders (Fig. 2G and H).

3.3. *Nfe2l1(f)-KO mice show reduced thermogenic mRNA expression and severe inflammation in the BAT*

To elucidate the molecular mechanisms underlying the cold intolerance and age-dependent BAT shrinking and whitening in *Nfe2l1*(f)-KO mice, we performed bulk RNA-seq of BAT from 4 weeks old female mice which show no significant differences in BAT mass between the two genotypes and 14–16 weeks old male mice independently. DEG analysis of data from 4-week-old females showed that there were 1778 up-regulated genes in KO, accounting for 8.29%, and 1248 down-

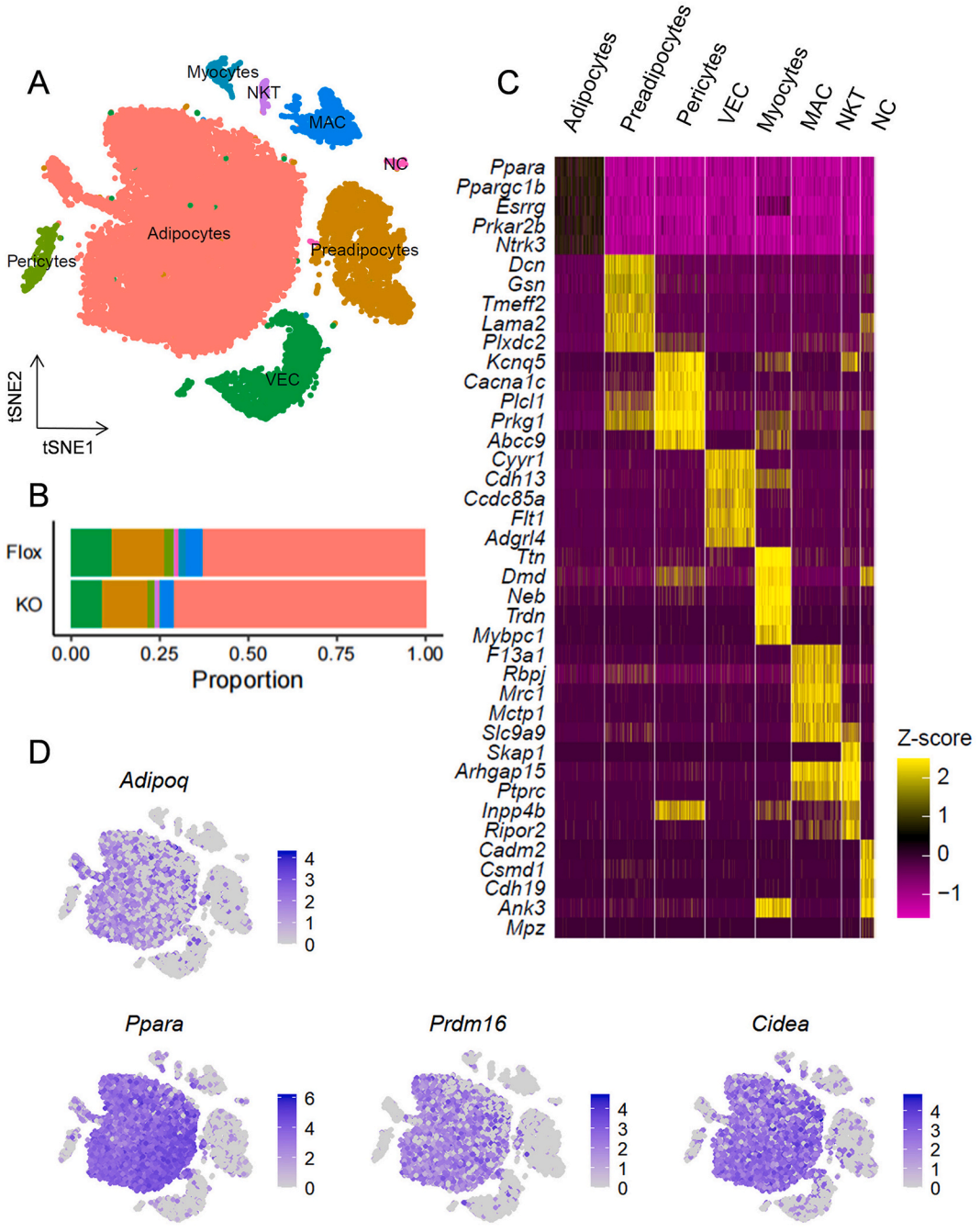

Fig. 6. Single-nucleus transcriptional analysis of BAT isolated from 4 weeks old female *Nfe2l1*(f)-KO and Flox mice. (A) t-distributed stochastic neighbor embedding (*t*-SNE) plot of 25,779 nuclei containing 14,153 Flox and 11,626 KO nuclei. (B) Heat map of marker genes for each nucleus type of BAT. Randomly sampled 500 nuclei of each nucleus type to show the top 5 marker genes. (C) Proportions of nucleus types in Flox and KO BAT. (D) Feature plots for *Ppara, Cidea, Adipoq* and *Prdm16*. Expression level (dot color) refers to the log normalized ratio of gene-expression reads, normalized to the sum of all reads within each nucleus type. (For interpretation of the references to color in this figure legend, the reader is referred to the Web version of this article.)

regulated genes, accounting for 5.82% of the detected genes (Fig. 3A). GSEA showed that down-regulated pathways include oxidative phosphorylation, tricarboxylic acid cycle, fatty acid metabolism, thermogenesis and proteasome, while up-regulated pathways were mainly closely related to immune and inflammatory response, such as graft versus host disease, cytokine-cytokine receptor interaction, NOD like receptor signaling pathway, and natural killer cell mediated cytotoxicity (Fig. 3B). In contrast, DEG analysis of data from 14 to 16 weeks males which had obvious whitening and shrinking of BAT in the KO mice (Fig. 2C and G) showed that there were 1088 up-regulated genes in KO, accounting for 5.29%, and 465 down-regulated genes, accounting for 2.26% (Fig. 3C). GSEA showed that the down-regulated pathways were generally consistent with those in 4 weeks old females, and the up-regulated pathways include natural killer cell-mediated cytotoxicity, as well as lysosome, antigen processing and presentation (APP), and B cell receptor signaling pathway (Fig. 3D). The venn diagram of down-regulated pathways showed that the two age/gender groups of mice shared multiple down-regulated pathways caused by *Nfe2l1* deficiency in adipocytes, mainly involving oxidative phosphorylation and thermogenesis (Fig. 3E). In contrast, as shown in Fig. 3F, the up-regulated pathways in *Nfe2l1*(f)-KO mice observed in both age/gender groups include autoimmune and inflammatory responses and natural killer cell-

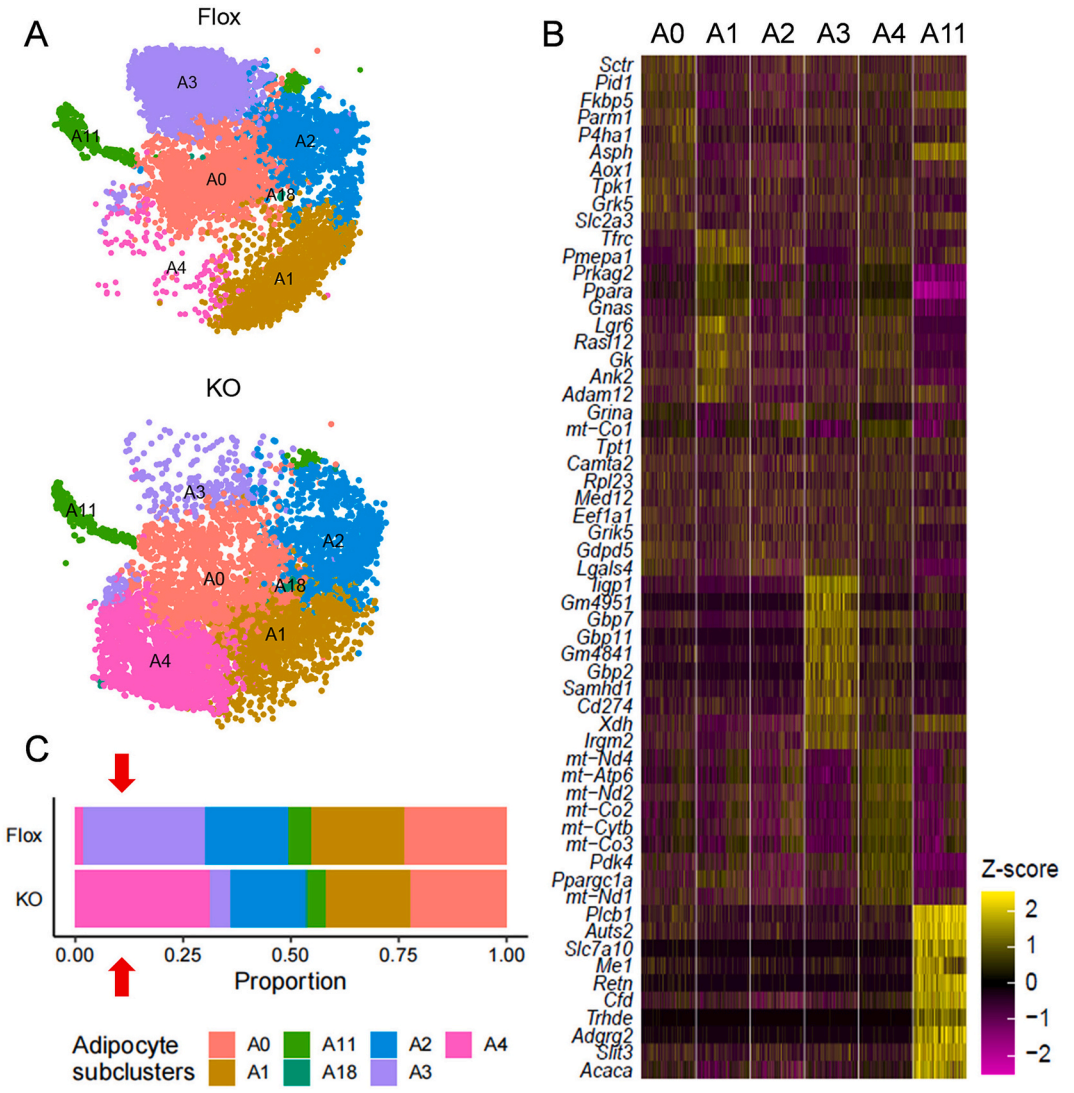

Fig. 7. The proportions of adipocyte subclusters are significantly different between Flox and KO groups. (A) *t*-SNE plots of adipocyte nuclei of Flox (upper) and KO (lower). A0, 1, 2, 3, 4, 11 and 18 refer to adipocyte subclusters (Seurat cluster number). (B) Heat map of signature genes for each subcluster of adipocyte nuclei. Randomly sampled 500 nuclei of each subcluster are shown for the top 10 signature genes. The number of A18 is too small to be displayed. (C) Adipocyte subcluster percentage compositions in Flox and KO nuclei.

mediated cytotoxicity. Furthermore, the up-regulated pathways differentially enriched in the two age/gender groups of mice are also related to inflammatory response and/or various RCD, such as necroptosis, suggesting that inflammatory response and subsequent RCD are the key processes mediating *Nfe2l1* deficiency-induced age-dependent BAT damage.

The results of bulk RNA-seq of BAT from 4 weeks old female and 14–16 weeks old male mice indicate that inflammation and subsequent immune responses are the most significant changes caused by *Nfe2l1* knockout in adipocytes. Thus, we performed RT-qPCR to verify the expression of upregulated DEGs that are enriched in the inflammatory response pathway, including adhesion G protein-coupled receptor E1 (*Adgre1*), *Cd68*, interferon γ (*Ifng*), interleukin 1β (*Il1b*), and pyroptosis-related factors, such as caspase 1 (*Casp1*), NLR family pyrin domain containing 3 (*Nlrp3*) and apoptosis-associated speck-like protein containing a CARD (*Pycard*). Indeed, the expression of all these genes in BAT was significantly increased in *Nfe2l1*(f)-KO mice compared to the Flox controls (Fig. 4A). In addition, immunohistochemical analyses of macrophage marker F4/80 clearly show that the BAT of *Nfe2l1*(f)-KO mice contains more hypertrophic adipocytes surrounded by F4/80-positive macrophages than those of Flox mice (Fig. 4B).

The most prominent function of BAC is to dissipate energy through uncoupled respiration to produce heat to contribute to body temperature maintenance and metabolic balance [26,27]. In line with the findings of phenotypic analyses and bulk RNA-seq of BAT, RT-qPCR analysis reveals that *Nfe2l1* deficiency in adipocytes resulted in significant decreases in the mRNA expression of genes related to BAC differentiation, thermogenesis, lipid metabolism and oxidation respiratory chain, including PR domain containing 16 (*Prdm16*), *Ucp1*, ELOVL fatty acid elongase 3 (*Elovl3*), *Elovl6*, carnitine palmitoyltransferase 1 B (*Cpt1b*), *Pparα*, cytochrome C oxidase subunit 8 B (*Cox8b*) and *Cox7a1* (Fig. 4C). Furthermore, the relative protein levels of UCP1, peroxisome proliferator-activated receptor-gamma coactivator-1 alpha (PGC1α), COX IV, NADH: ubiquinone oxidoreductase subunit S4 (NDUFS4), oxidative phosphorylation (OXPHOS), mitochondrial fission protein 1 (FIS1) and optic atrophy 1 mitochondrial dynamin like GTPase (OPA1) were markedly lower in BAT of *Nfe2l1*(f)-KO mice than those in Flox control mice (Fig. 4D and E), suggesting that adipocyte-specific ablation of *Nfe2l1* impairs the function of mitochondria in BAT. In addition, transmission electron microscopy showed that *Nfe2l1*(f)-KO mice have considerably larger lipid droplets (LDs) in their BAT compared to Flox control (Fig. 4F). In addition, there were many swollen mitochondria

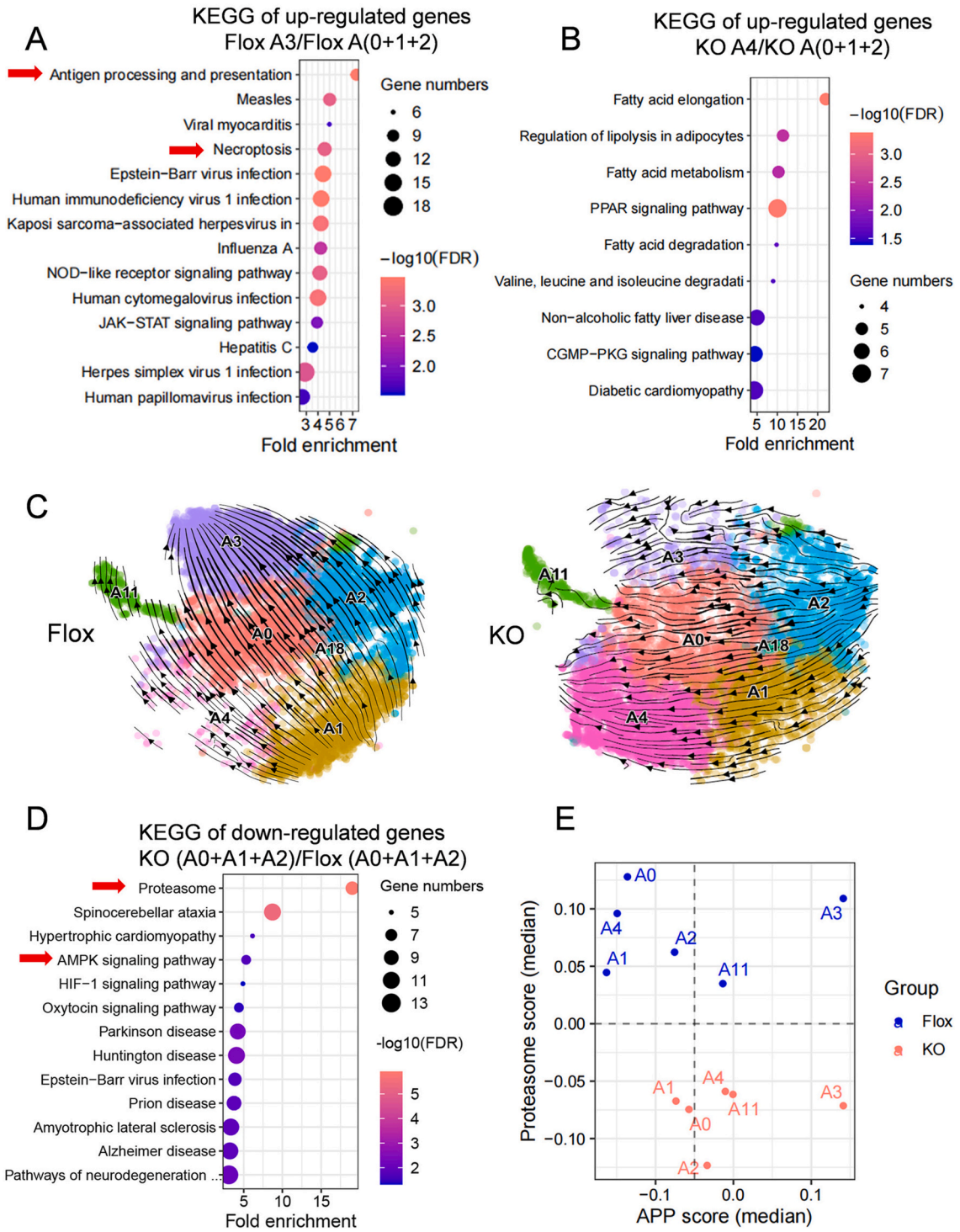

Fig. 8. Characterization of adipocyte subclusters in Flox and KO nuclei. (A and B) Kyoto encyclopedia of genes and genomes (KEGG) pathway enrichment analysis of A3 (A) and A4 (B) signature genes compared to A0, A1 and A2 combined subclusters in Flox (A) and KO (B) nuclei, respectively. The bubble chart of up-regulated genes is displayed. (C) RNA velocity analysis showing dynamic transitions among adipocyte nuclei subclusters in Flox (left panel) and KO (right panel) mice. (D) The bubble chart of down-regulated genes enriched in the KEGG pathway enrichment analysis of A0, A1 and A2 combined subclusters of KO nuclei compared to those of Flox. (E) Scatter plot of antigen processing and presentation (APP) score median vs. proteasome score median of adipocyte subclusters.

with disorganized and fractured cristae in the BAT of *Nfe2l1*(f)-KO mice (Fig. 4F).

3.4. *Down-regulated expression of lipolytic genes is involved in the BAT inflammation in Nfe2l1(f)-KO mice*

Our previous studies, mainly in *Nfe2l1*(f)-KO mice, have demonstrated that NFE2L1-dependent expression of multiple lipolytic genes is crucial for energy homeostasis and plasticity of WAT. *Nfe2l1*(f)-KO mice express reduced levels of multiple lipolytic genes in adipocytes, leading to adipocyte hypertrophy followed by severe inflammation, pyroptosis and thereby diminished WAT mass [11,18–21]. To test the hypothesis that *Nfe2l1* deficiency may deteriorate BAT by down-regulating lipolytic genes, we measured the expression of multiple key

lipolytic genes in BAT of *Nfe2l1*(f)-KO. As shown in Fig. 5A–C, adipocyte-specific *Nfe2l1* deficiency led to significantly reduced mRNA and/or protein expression of multiple lipolytic genes, including patatin-like phospholipase domain containing 2 (PNPLA2)/adipocyte triglyceride lipase (ATGL), hormone-sensitive lipase (HSL) and monoacylglycerol lipase (MGL) and perilipin 1 (PLIN1). Keeping in line with the repressed expression of the lipolytic genes at mRNA and protein levels, the basal and CL316243, a β3-adrenergic agonist promoting lipolysis via a post-translational mechanism, stimulated lipolytic activity were significantly lower in the BAT of *Nfe2l1*(f)-KO mice compared with those of Flox mice (Fig. 5D and E). To test the hypothesis that the BAT phenotype of *Nfe2l1*(f)-KO mice, BAT inflammation in particular, is attributed, at least in part, to decreased lipolytic activity in BAC, we investigated the effect of CL316243 on BAT inflammation in 4 weeks old *Nfe2l1*(f)-KO mice. As shown in Fig. 5F–H, 7 days of CL316243 treatment substantially changed the BAT into darker brown, reduced lipid accumulation and slightly increased the mass of BAT in both genotypes of mice. Interestingly, CL316243 treatment showed no significant effect on the expression of BAT marker genes in both genotypes (Fig. 5I). However, *Nfe2l1*(f)-KO and Flox mice showed opposite effects with inflammatory gene expression in response to the treatment. While CL316243 treatment increased the mRNA expression of multiple inflammatory genes in the BAT of Flox control mice, the same treatment significantly alleviated the induction of the genes caused by *Nfe2l1* deficiency, indicating that reduced lipolytic activity is involved in the BAT inflammation in *Nfe2l1*(f)-KO mice.

3.5. snRNA-seq reveals altered cellular heterogeneity and dynamics of BAT of Nfe2l1(f)-KO mice

To understand the distinct roles of NFE2L1 in BAC at higher resolution, we next performed snRNA-seq of BAT isolated from young female mice housed at room temperature (Supplementary Fig. S3). After quality control, there were 14,153 and 11,626 nuclei in Flox and KO groups, respectively, selected for dimension reduction, clustering, visualization, and cluster identification. As shown in Supplementary Figs. S4 and 20 subgroups of nuclei numbered 0–19 were clustered, among which 8 main nuclear types, namely adipocytes, preadipocytes, macrophages (MAC), natural killer/T cells (NK/T), vascular endothelial cells (VEC), pericytes, myocytes and nerve cells (NC), were identified (Fig. 6A) based on their feature markers (Supplementary Fig. S5). Among the 8 nuclear types, the proportion of adipocytes is 71.12% in KO group, which is significantly higher than that of Flox control (63.10%). Other nuclear types except NKT cluster showed substantially decreased proportions in KO group relative to Flox control (Fig. 6B, Supplementary Table S3). To further verify the identity of the adipocyte cluster, we compared the top 5 marker genes among the 8 nuclear types identified. As shown in Fig. 6C, the heat map of their marker genes showed that the adipocyte cluster is distinct from all other nuclear types. In addition, several classical BAC markers, including *Ppara, Prdm16, Cidea* and *Adipoq*, were found to express selectively in the adipocyte cluster identified (Fig. 6D).

To investigate the molecular details underlying *Nfe2l1* deletion-induced BAC malfunction, the cluster of adipocyte nuclei was further divided into 7 subclusters, namely A0, A1, A2, A3, A4, A11 and A18 (Fig. 7A) based on their feature markers (Fig. 7B). A18 subcluster was not shown here and in subsequent analyses due to its small size (Supplementary Table S4). The subcluster number adopts their initial cluster seurat number before identification (Supplementary Fig. S4), for example, A0 represents the adipocyte 0 subcluster. The proportions of A0, A1, A2 and A11 subclusters were only marginally decreased in KO relative to Flox nuclei. In contrast, A3 subcluster displayed a marked decrease from 28.18% to 4.63%, while A4 cluster displayed a dramatic increase from 1.89% to 31.28% in the KO adipocytes compared to those of Flox mice (Fig. 7C, Supplementary Table S4).

The top 10 characteristic genes that clearly distinguished A3 from other subclusters are *Iigp1, Gm4951, Gbp7, Gbp11, Gm4841, Gbp2, Samhd1, Cd274, Irgm2* and *Xdh,* which are all related to immune and inflammatory responses (Fig. 7B). In contrast, A4 subcluster highly expressed mitochondrial biogenesis-related genes, including *mt-Nd4, mt-Atp6, mt-Nd2, mt-Co2, mt-Cytb, mt-Co3, Pdk4, Ppargc1α, mt-Nd1*, indicating that these cells have activated mitochondrial biogenesis. Of note, the characteristics of A11 with high expression of *Plcb1, Auts2, Slc7a10, Me1, Retn, Cfd, Trhde, Adgrg2, Slit3* and *Acaca* showed a similar mRNA profiling to a new type of BAC identified in a recent study [7], which specifically expresses *Cyp2e1* and regulates thermogenesis (Supplementary Fig. S6).

Given that the proportions of A0, A1 and A2 between genotypes are relatively comparable and there was little heterogeneity among these subclusters (Fig. 7B), we assumed that these three subclusters may represent classic thermogenic BAC. To further characterize the A3 subcluster, a DEG analysis was performed between A3 and the combined subclusters of A0, A1 and A2 (A0+A1+A2) using the data from Flox nuclei, followed by a KEGG enrichment analysis using genes with significant difference between the 2 subclusters. As illustrated in Fig. 8A, the up-regulated genes in A3 relative to A0+A1+A2 combined subcluster in Flox nuclei involve APP, necroptosis and other pathways related to immune and inflammatory responses. In contrast, the down-regulated genes in A3 include glucagon signaling pathway, fatty acid metabolism and the pathways related to metabolism (Supplementary Fig. S7).

To characterize the A4 subcluster, a DEG analysis was performed between A4 and A0+A1+A2 combined subcluster using the data from KO nuclei, followed by a KEGG enrichment analysis of significantly changed genes. As shown in Fig. 8B, the up-regulated genes in A4 relative to A0+A1+A2 combined subcluster in KO nuclei involve fatty acid metabolism, regulation of lipolysis in adipocytes, and PPAR signaling pathway. However, there were no enriched pathways identified using the down-regulated genes in A4 relative to A0+A1+A2 combined subcluster in KO nuclei. The aforementioned data suggests that A4 may be a subpopulation of BAC that emerged as a compensatory mechanism with partial BAC function in the absence of *Nfe2l1*.

To further understand the mechanism by which *Nfe2l1* deficiency impairs the heterogeneity of BAT, an RNA velocity analysis, which provides an overview of the transcriptional transient dynamic changes in cells, was conducted. As shown in Fig. 8C, the result of Flox nuclei suggests that A3 may be the terminally differentiated adipocytes, which is in line with the suggested function above that A3 is a type of BAC of very low thermogenic and metabolic capacity and is close to cell death. Compared with Flox, the transient dynamic direction of transcription of KO nuclei has an overall direction towards A4 subpopulation.

Because A3 and A4 subclusters show clear cell type diversity and their proportions in adipocytes vary dramatically between genotypes, any analysis related to classical BAC may be confounded by the inclusion of A3 and/or A4 subclusters. Thus, we focused on A0+A1+A2 subclusters, which account for over 58% of adipocyte clusters (Supplementary Table S4), and compared the gene expression between Flox and KO nuclei. As shown in Fig. 8D, enrichment analysis of down-regulated genes reveals that proteasome pathway and AMPK signaling pathway are crucial in the combined subclusters of KO relative to Flox nuclei. In contrast, the up-regulated genes involve lipid metabolism, FFA metabolism in particular (Supplementary Fig. S9). We further calculated proteasome, AMPK, APP and necroptosis scores for each subcluster (Supplementary Fig. S10) and then scatter plotted using the median scores of the subclusters (Fig. 8E, Supplementary Fig. S11). The results show that the score of proteasome, AMPK, APP or necroptosis used either individually or in combination can distinguish various adipocyte subclusters of KO from those of Flox mice, highlighting that the pathways are functionally impaired by *Nfe2l1* deficiency in BAC.

4. Discussion

In the present study, we performed a detailed phenotypic and

functional characterization of *Nfe2l1*(f)-KO mice with an emphasis on BAT to understand the molecular details underlying the physiological roles of NFE2L1 in BAC. In line with the earlier findings from BAC-specific *Nfe2l1* knockout mice [9], we found that *Nfe2l1*(f)-KO mice display age-dependent whitening and shrinking of BAT, which is characterized by accumulation of large monocellular LDs in BAC and reduction of BAT mass. In addition, the BAT of *Nfe2l1*(f)-KO mice displayed decreased expression of genes involved in lipolysis, proteasome, and mitochondria, with subsequent induction of pro-inflammatory genes. Bulk RNA-seq of BAT from *Nfe2l1*(f)-KO mice of different ages and/or genders demonstrated that NFE2L1 is crucial in proteostasis, lipid metabolism, BAC thermogenesis and subsequent cell fate determination. SnRNA-seq of BAT demonstrated that deficiency of *Nfe2l1* in adipocytes induces aberrant expression of a variety of genes involved in lipid metabolism, proteasome, mitochondrial stress, inflammatory response, antigen processing and presentation, and RCD in distinct subpopulations of BAC. These findings reveal a novel mechanism that NFE2L1 serves as a vital transcriptional regulator in controlling lipid metabolic homeostasis and thus BAC dynamics and heterogeneity.

BAC thermogenesis is an important component of energy production and expenditure and facilitates cold tolerance and acclimation [2,27,28]. Upon cold exposure, the sympathetic nervous system releases catecholamines, which bind mainly β3-adrenergic receptor (β3-AR) to activate the protein kinase A (PKA) pathway in adipocytes [3,29,30]. Since lipolysis plays an essential role in thermogenesis, inhibition of intracellular lipolysis suppresses cold-induced NST in BAT [31]. Lipolysis involves enzymatic breakdown of TAG by lipases, including ATGL, HSL and MGL, and is controlled by a nutritionally-sensitive signal transduction cascade containing multiple kinases and LD proteins, including PLIN1 [32,33]. PLIN1 coats LDs in adipocytes and is involved in LD formation, triglyceride storage, and lipolysis. Following the activation of PKA, phosphorylated PLIN1 modulates the activity of ATGL by controlling the access of αβ hydrolase domain-containing protein 5 to ATGL [34,35], and the activity of HSL by providing a docking site on lipid droplets for lipase access that promote lipolysis [36,37]. In addition, cold-induced expression of PLIN1 is tightly associated with lipid mobilization in thermogenesis cells [38]. Previous studies demonstrated that *Atgl*-deficient mice develop brown adipocytes hypertrophy and BAT inflammation [25]. Consistently, the BAC of *Hsl*-KO mice were significantly enlarged [39]. In the current study, we found that deficiency of *Nfe2l1* results in dramatically reduced expression of multiple lipolytic genes, including *Atgl*, *Hsl* and *Plin1*, at mRNA and protein levels in BAT. In addition, the basal and CL316243-stimulated lipolytic activities were diminished in the *Nfe2l1*(f)-KO BAT. The compromised lipolytic activity and subsequent decreased thermogenesis coupled with impaired proteasome function result in lipid accumulation, ER stress, ensuing inflammatory response and associated RCD in BAT. Interestingly, the BAT inflammation in *Nfe2l1*(f)-KO mice can be substantially rescued by a subacute treatment with CL316243, a β3-adrenergic agonist promoting lipolysis via a post-translational mechanism, at least in young mice, highlighting that the down-regulated lipolytic gene expression is one of the primary mechanisms underlying the BAT dysfunction in the absence of *Nfe2l1*. Nevertheless, β3-AR is emerging as an appealing target for novel pharmacological approaches in treating several diseases, including metabolic disorders [30]. CL316243, one of the first-generation β3-AR agonists, is highly selective and potent, and has been shown in rodent models to be an effective agent for treating obesity and Type II diabetes [30]. Thus, our current study provides additional novel experimental evidence supporting that β3-AR agonists, including CL316243, could be a valuable approach to treating BAT dysfunction.

An abundance of data have shown that β3-AR-PKA signaling-mediated phosphorylation and other posttranslational mechanisms play critical roles in regulating the activity and/or function of various lipolytic proteins, including ATGL, HSL, and PLIN1 [3]. However, the promoter activities of these key lipolytic genes and associated transcriptional cascades have not been fully characterized. In the current study, although we have provided no evidence that the key lipolytic genes are direct downstream transcriptional targets of NFE2L1, RNA profiles of BAC/BAT of current study along with previous findings on the mRNA expression of lipolytic genes in WAC/WAT [11,18–21] highly suggest that NFE2L1 is one of the key factors that control the transcription of the lipolytic genes. In addition, emerging evidence indicates that multiple factors, PPARγ in particular, are involved in the transcriptional activation or repression of the key lipolytic genes [40,41]. Interestingly, our previous mechanistic studies in 3T3-L1 cells indicated that NFE2L1 regulates the expression of *Pparγ2* in an isoform-specific manner [21]. Thus, it is highly possible that NFE2L1 coordinates with other nuclear factors/receptors to control the transcription of the lipolytic genes. Given that the gene structures and promoter activities of the key lipolytic genes, ATGL, HSL, and PLIN1 in particular, have not been fully characterized, the molecular details underlying the transcriptional regulation of the key lipolytic genes by NFE2L1 warrants further investigation.

It has been well documented that hypertrophic adipocytes are prone to developing organelle dysfunction, such as ER stress, mitochondrial dysfunction, and activation of the NLRP3 inflammasome pathway [42,43], suggesting that hypertrophically stressed adipocytes undergo pyroptotic cell death and initiate an inflammatory response. Given that BAC in *Nfe2l1*(f)-KO mice exhibit noticeable hypertrophy, we reason that the BAT inflammation is the secondary consequence of hypertrophic stress. Regarding the roles of proteasome in BAC, it has been reported that ubiquitin proteins are highly abundant in BAT and regulated by cold, but they are dispensable for BAC proteostasis and thermogenesis [17,44]. Loss of *Psme1* and/or *Psme4* did not impair BAC development or activation, suggesting that proteasomes are required neither for brown adipogenesis nor NST [45]. In contrast, Bartelt et al. showed that NFE2L1 functions as a critical driver in BAT thermogenic adaption to cold or obesity by providing proteometabolic quality control [9]. Thus, a more complete understanding of the systemic as well as adipocyte-specific roles of NFE2L1-proteasome cascade could improve treatment options of various metabolic disorders.

A proper mitochondrial function is required for normal metabolism of thermogenic cells. Reduction of mitochondrial mass and oxidative capacity induces defects in adaptive thermogenesis [46]. In our study, deficiency of *Nfe2l1* in adipocytes causes an obvious reduction of mitochondria mass and dysfunction of oxidative phosphorylation, indicating that NFE2L1 is involved in mitochondrial dynamics and homeostasis. Several studies have proposed that mitochondria and LDs might closely collaborate, and the connectivity between LDs and mitochondria would facilitate FFA transfer to the mitochondrion during lipolysis [47,48]. Moreover, effective lipolytic stimulation to trigger fatty acid β-oxidation requires the expression of PLIN1 [49]. In our study, we found that *Nfe2l1*(f)-KO mice have swelling mitochondria in the BAC and aberrant expression of mitochondrial genes including dramatic downregulation of PLIN1. Therefore, we speculate that the absence of *Nfe2l1* reduces PLIN1 expression and thus mitochondria–LD interaction, leading to BAC hypertrophy and subsequent damages to BAT.

Although it has been shown that NFE2L1 is essential for adaptive thermogenesis in BAC [9], the effects of *Nfe2l1* deletion at single cell level have not been elucidated. Revealing the cellular heterogeneity and dynamics of BAT is critical to understanding and targeting this unique tissue in treating metabolic diseases. Here, the cell composition analysis of snRNA-seq data showed that the proportion of total adipose nuclei in the KO group (71.12%) was higher than that in the Flox group (63.10%), while the proportion of preadipocyte nuclei in the KO group (12.87%) was lower than that in the Flox mice (15.12%). These alterations suggest that the differentiation from preadipocytes into adipocytes may be accelerated in KO mice. Our previous studies [21] found that the stromal vascular fraction of cells isolated from WAT of *Nfe2l1*(f)-KO mice display augmented adipogenesis characterized by elevated mRNA and protein expression of adipogenic markers and lipid accumulation. Clearly, our

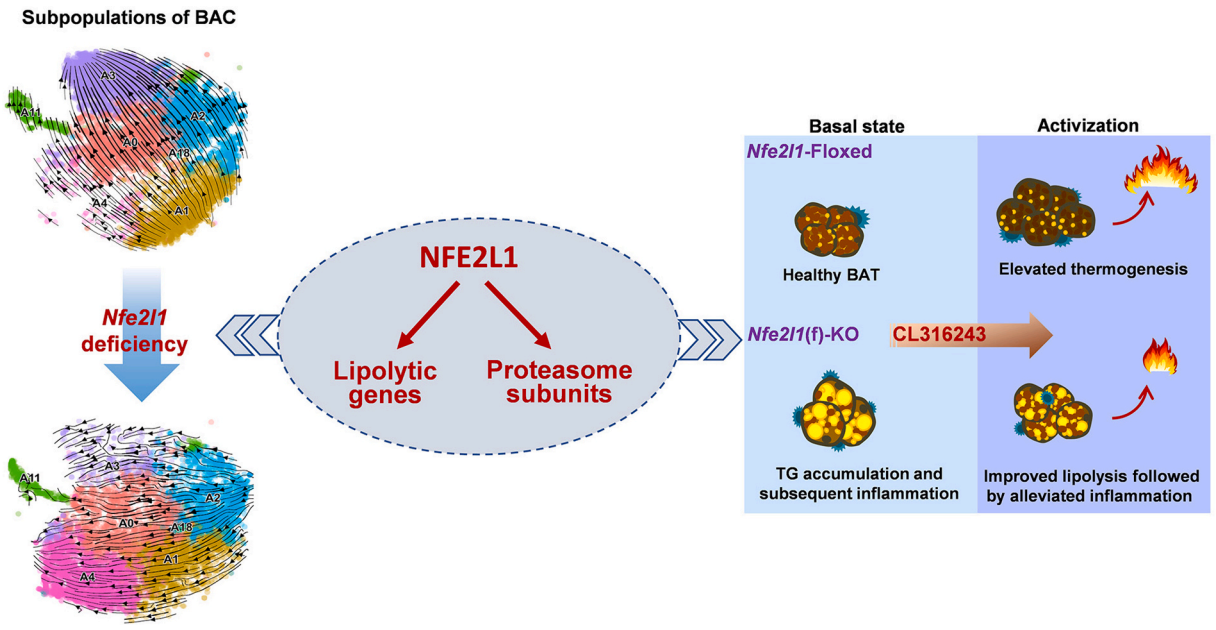

Fig. 9. The potential mechanisms underlying the impairments of BAT in *Nfe2l1*(f)-KO mice. The expression of multiple key lipolytic and proteasome subunit genes is, at least in part, dependent on NFE2L1. Ablation of *Nfe2l1* in adipocytes may result in diminished lipolysis and disrupted proteometabolic quality control in BAC. As a result, on the one hand, the absence of *Nfe2l1* in BAC modifies the direction of transcriptional dynamics and disrupts BAC differentiation, cell fate determination and thus cellular dynamics and heterogeneity; on the other hand, *Nfe2l1*(f)-KO mice are prone to lipid accumulation in BAC and subsequent pro-inflammatory response and RCD, which may cause BAT whitening and impaired thermogenesis. CL316243 treatment, which increases the lipolytic activity of the down-regulated lipolytic enzymes of *Nfe2l1*(f)-KO BAT via a post-translational mechanism, partially alleviates the BAT inflammation of *Nfe2l1*(f)-KO mice, highlighting the crucial role of NFE2L1 in lipolysis and BAC homeostasis.

previous findings *in vitro* are in line with what we found in the BAT, whereas a more detailed investigation is needed to verify the involvement of NFE2L1 in adipogenic differentiation of BAC.

By focusing on BAC subpopulations, we found that among the 6 subpopulations, A3, A4 and A11 showed great differences between the Flox and KO mice. The characteristics of A11 (Supplementary Fig. S6) are highly consistent with the mRNA profiling of a type of BAC that specifically expresses *Cyp2e1* and regulates thermogenesis [7]. These primary findings highlight that our results are in agreement with the published data and thus reliable. In KO mice, A3 subpopulation is dramatically reduced while A4 expanded. We characterized and identified A3 as a non-classical BAC with low thermogenesis activity, low glucose and lipid metabolism and high inflammatory RCD gene expression. Song et al. [6] has shown that low- and high-thermogenic brown adipocyte subpopulations coexist in murine adipose tissue. Using their published dataset, we found that the characteristic genes of A3, such as *Gbp2, Gbp7, Irf1, Xdh,* and *Iigp1*, were expressed at certain levels in the low-thermogenic nonclassical BAC, but not in the high-thermogenic classical BAC (Supplementary Fig. S8), suggesting that the A3 subpopulation we identified here represents a subgroup of non-classical low-thermogenic BAC. Together with the mRNA signatures of the subcluster (augmented APP, necroptosis and other pathways related to immune and inflammatory responses; decreased glucagon signaling and the pathways related to metabolism), we speculate that the A3 subpopulation may be at a stage of exhaustion and/or aging and is prone to RCD. Therefore, the A3 subcluster was almost diminished in KO adipocytes, since most of the A3 cells cannot survive in the microenvironment induced by *Nfe2l1* deficiency. Regarding the enriched A4 subpopulation in KO group, we surmise that it is a compensatory state with insufficient functionality, which is echoed by the aberrant expression of mitochondrial and lipid metabolism genes and increased APP and necroptosis scores.

There are some limitations in our current study. First, the ablation of *Nfe2l1* was accomplished by employing the *adipoq*-Cre, which targets mature adipocytes, including BAC and WAC. It may not be rigorous to target such a large population of cells because it may lead to altered systemic metabolism, which in turn impacts the function of BAC [50]. Therefore, it is of great importance to use multiple models with genetic modifications of *Nfe2l1* in future studies to draw more unbiased conclusions on *Nfe2l1* in BAT function; Second, we found there are lack of reliable approaches to further verify the key findings related to those interesting subpopulations of BAC identified in snRNA-seq. Our preliminary characterization of those subpopulations of BAC warrants further investigations to understand their respective functions in BAT homeostasis. Third, given that the *Nfe2l1* gene may be transcribed in multiple alternatively-spliced forms resulting in multiple protein isoforms [11], the isoform-specific role of NFE2L1 in BAC biology still needs detailed studies. Forth, the molecular details underlying the transcriptional regulation of lipolytic genes have not been established in BAC, even though we have provided multiple lines of evidence that *Nfe2l1* deficiency results in decreased expression of those key lipolytic factors, including ATGL, HSL, and PLIN1. Nevertheless, considering that human *NFE2L1* gene contains many SNPs, which might affect the expression and function of different isoforms of NFE2L1, the physiological significance of NFE2L1 in human health also merits further investigation.

In summary, our studies provide novel insights into the mechanistic details in the critical transcriptional regulatory roles of NFE2L1 in BAC. We characterized, for the first time, the heterogeneity, dynamics, and homeostasis of BAC caused by *Nfe2l1* deletion at the single-nucleus transcriptome level. We scenarize that absence of *Nfe2l1* in adipocytes results in diminished transcription of lipolysis and proteasome genes, leading to altered direction of the transcription dynamics in BAC and thus disrupting BAC differentiation and cell fate. Therefore, *Nfe2l1*(f)-KO mice are prone to lipid accumulation in BAC, which may trigger subsequent pro-inflammatory response and induce inflammation-related RCD leading to BAT whitening and impaired thermogenesis (Fig. 9). Taken the findings from our previous studies on WAT [11, 18–21] together, we conclude that deletion of *Nfe2l1* in adipocytes results in reduced lipolysis coupled with augmented lipogenesis leading to

lipid overload in WAC and BAC and subsequent cell damages. Thus, our findings provide new perspectives on how NFE2L1-dependent lipolytic and proteasome activity determine the dynamic and plasticity of BAC and BAT heterogeneity and homeostasis. Considering that NFE2L1 functions as a vital transcriptional regulator in a variety of cell metabolism, an understanding of the pleiotropic functions of NFE2L1 in adipocytes may help identify NFE2L1 in adipose tissues as a therapeutic target for metabolic disorders, such as obesity and diabetes.

Declaration of competing interest

The authors declare that they have no known competing financial interests or personal relationships that could have appeared to influence the work reported in this paper.

Data availability

Data will be made available on request.

Acknowledgements

This research was funded by the National Natural Science Foundation of China 81830099 (J.P.), 82020108027 (J.P.), 82173510 (Y.H.); Innovation Team Support of China Medical University (CXTD2022004); High-level Talents Support Foundation of China Medical University 2400022032 (Y.X.), 2400022052 (H.W.), 2400022054 (J.F.). The authors have no conflicting financial interests.

Appendix A. Supplementary data

Supplementary data to this article can be found online at https://doi.org/10.1016/j.redox.2023.102879.

References

[1] X. Zhang, S. Ha, H.C. Lau, J. Yu, Excess body weight: novel insights into its roles in obesity comorbidities, Semin. Cancer Biol. 92 (2023) 16–27, https://doi.org/10.1016/j.semcancer.2023.03.008.
[2] S.S. Michurina, I.S. Stafeev, M.Y. Menshikov, Y.V. Parfyonova, Mitochondrial dynamics keep balance of nutrient combustion in thermogenic adipocytes, Mitochondrion 59 (2021) 157–168, https://doi.org/10.1016/j.mito.2021.05.001.
[3] A. Sakers, M.K. De Siqueira, P. Seale, C.J. Villanueva, Adipose-tissue plasticity in health and disease, Cell 185 (2022) 419–446, https://doi.org/10.1016/j.cell.2021.12.016.
[4] C. Bienboire-Frosini, et al., The role of Brown adipose tissue and energy metabolism in mammalian thermoregulation during the perinatal period, Animals : Open Access J. MDPI 13 (2023), https://doi.org/10.3390/ani13132173.
[5] Y. Oguri, S. Kajimura, Cellular heterogeneity in brown adipose tissue, J. Clin. Invest. 130 (2020) 65–67, https://doi.org/10.1172/JCI133786.
[6] A. Song, et al., Low- and high-thermogenic brown adipocyte subpopulations coexist in murine adipose tissue, J. Clin. Invest. 130 (2020) 247–257, https://doi.org/10.1172/JCI129167.
[7] W. Sun, et al., snRNA-seq reveals a subpopulation of adipocytes that regulates thermogenesis, Nature 587 (2020) 98–102, https://doi.org/10.1038/s41586-020-2856-x.
[8] Y. Zhang, Y. Xiang, Molecular and cellular basis for the unique functioning of Nrf1, an indispensable transcription factor for maintaining cell homoeostasis and organ integrity, Biochem. J. 473 (2016) 961–1000, https://doi.org/10.1042/BJ20151182.
[9] A. Bartelt, et al., Brown adipose tissue thermogenic adaptation requires Nrf1-mediated proteasomal activity, Nat. Med. 24 (2018) 292–303, https://doi.org/10.1038/nm.4481.
[10] I.L. Lemmer, N. Willemsen, N. Hilal, A. Bartelt, A guide to understanding endoplasmic reticulum stress in metabolic disorders, Mol. Metabol. 47 (2021), 101169, https://doi.org/10.1016/j.molmet.2021.101169.
[11] S. Ren, et al., The roles of NFE2L1 in adipocytes: structural and mechanistic insight from cell and mouse models, Redox Biol. 44 (2021), 102015, https://doi.org/10.1016/j.redox.2021.102015.
[12] E.K. Speliotes, et al., Association analyses of 249,796 individuals reveal 18 new loci associated with body mass index, Nat. Genet. 42 (2010) 937–948, https://doi.org/10.1038/ng.686.
[13] Y. Hirotsu, et al., Transcription factor NF-E2-related factor 1 impairs glucose metabolism in mice, Gene Cell. 19 (2014) 650–665, https://doi.org/10.1111/gtc.12165.
[14] P. Patel, V. Selvaraju, J.R. Babu, X. Wang, T. Geetha, Racial disparities in methylation of NRF1, FTO, and LEPR gene in childhood obesity, Genes 13 (2022), https://doi.org/10.3390/genes13112030, 2030.
[15] A. Rushing, E.C. Sommer, S. Zhao, E.K. Po'e, S.L. Barkin, Salivary epigenetic biomarkers as predictors of emerging childhood obesity, BMC Med. Genet. 21 (2020) 34, https://doi.org/10.1186/s12881-020-0968-7.
[16] S. Wahl, et al., Epigenome-wide association study of body mass index, and the adverse outcomes of adiposity, Nature 541 (2017) 81–86, https://doi.org/10.1038/nature20784.
[17] N. Willemsen, I. Arigoni, M. Studencka-Turski, E. Kruger, A. Bartelt, Proteasome dysfunction disrupts adipogenesis and induces inflammation via ATF3, Mol. Metabol. 62 (2022), 101518, https://doi.org/10.1016/j.molmet.2022.101518.
[18] Y. Hou, et al., Adipocyte-specific deficiency of Nfe2l1 disrupts plasticity of white adipose tissues and metabolic homeostasis in mice, Biochem. Biophys. Res. Commun. 503 (2018) 264–270, https://doi.org/10.1016/j.bbrc.2018.06.013.
[19] S. Ren, et al., Protracted rosiglitazone treatment exacerbates inflammation in white adipose tissues of adipocyte-specific Nfe2l1 knockout mice, Food Chem. Toxicol. : Int. J. publ. Br. Ind. Biol. Res. Assoc. 146 (2020), 111836, https://doi.org/10.1016/j.fct.2020.111836.
[20] Z. Wang, et al., CL316243 treatment mitigates the inflammation in white adipose tissues of juvenile adipocyte-specific Nfe2l1 knockout mice, Free Radic. Biol. Med. 165 (2021) 289–298, https://doi.org/10.1016/j.freeradbiomed.2021.01.043.
[21] P. Xue, et al., Long isoforms of NRF1 negatively regulate adipogenesis via suppression of PPARgamma expression, Redox Biol. 30 (2020), 101414, https://doi.org/10.1016/j.redox.2019.101414.
[22] M. Ohtsuji, et al., Nrf1 and Nrf 2 play distinct roles in activation of antioxidant response element-dependent genes, J. Biol. Chem. 283 (2008) 33554–33562, https://doi.org/10.1074/jbc.M804597200.
[23] A. Mehlem, C.E. Hagberg, L. Muhl, U. Eriksson, A. Falkevall, Imaging of neutral lipids by oil red O for analyzing the metabolic status in health and disease, Nat. Protoc. 8 (2013) 1149–1154, https://doi.org/10.1038/nprot.2013.055.
[24] P. Xue, et al., Prolonged inorganic arsenite exposure suppresses insulin-stimulated AKT S473 phosphorylation and glucose uptake in 3T3-L1 adipocytes: involvement of the adaptive antioxidant response, Biochem. Biophys. Res. Commun. 407 (2011) 360–365, https://doi.org/10.1016/j.bbrc.2011.03.024.
[25] V. Bergen, M. Lange, S. Peidli, F.A. Wolf, F.J. Theis, Generalizing RNA velocity to transient cell states through dynamical modeling, Nat. Biotechnol. 38 (2020) 1408–1414, https://doi.org/10.1038/s41587-020-0591-3.
[26] Z. Zhang, et al., Non-shivering thermogenesis signalling regulation and potential therapeutic applications of Brown adipose tissue, Int. J. Biol. Sci. 17 (2021) 2853–2870, https://doi.org/10.7150/ijbs.60354.
[27] F. Shamsi, C.H. Wang, Y.H. Tseng, The evolving view of thermogenic adipocytes - ontogeny, niche and function, Nat. Rev. Endocrinol. 17 (2021) 726–744, https://doi.org/10.1038/s41574-021-00562-6.
[28] D.P. Blondin, Human thermogenic adipose tissue, Curr. Opin. Genet. Dev. 80 (2023), 102054, https://doi.org/10.1016/j.gde.2023.102054.
[29] J. Liu, Y. Wang, L. Lin, Small molecules for fat combustion: targeting obesity, Acta Pharm. Sin. B 9 (2019) 220–236, https://doi.org/10.1016/j.apsb.2018.09.007.
[30] G. Schena, M.J. Caplan, Everything you always wanted to know about beta(3)-AR * (* but were afraid to ask), Cells 8 (2019), https://doi.org/10.3390/cells8040357.
[31] D.P. Blondin, et al., Inhibition of intracellular triglyceride lipolysis suppresses cold-induced Brown adipose tissue metabolism and increases shivering in humans, Cell Metabol. 25 (2017) 438–447, https://doi.org/10.1016/j.cmet.2016.12.005.
[32] A. Yang, E.P. Mottillo, Adipocyte lipolysis: from molecular mechanisms of regulation to disease and therapeutics, Biochem. J. 477 (2020) 985–1008, https://doi.org/10.1042/BCJ20190468.
[33] G.F. Grabner, H. Xie, M. Schweiger, R. Zechner, Lipolysis: cellular mechanisms for lipid mobilization from fat stores, Nat. Metab. 3 (2021) 1445–1465, https://doi.org/10.1038/s42255-021-00493-6.
[34] V. Subramanian, et al., Perilipin A mediates the reversible binding of CGI-58 to lipid droplets in 3T3-L1 adipocytes, J. Biol. Chem. 279 (2004) 42062–42071, https://doi.org/10.1074/jbc.M407462200.
[35] A. Sahu-Osen, et al., CGI-58/ABHD5 is phosphorylated on Ser 239 by protein kinase A: control of subcellular localization, J. Lipid Res. 56 (2015) 109–121, https://doi.org/10.1194/jlr.M055004.
[36] H. Miyoshi, et al., Perilipin promotes hormone-sensitive lipase-mediated adipocyte lipolysis via phosphorylation-dependent and -independent mechanisms, J. Biol. Chem. 281 (2006) 15837–15844, https://doi.org/10.1074/jbc.M601097200.
[37] C. Sztalryd, D.L. Brasaemle, The perilipin family of lipid droplet proteins: gatekeepers of intracellular lipolysis, Biochim. Biophys. Acta Mol. Cell Biol. Lipids 1862 (2017) 1221–1232, https://doi.org/10.1016/j.bbalip.2017.07.009.
[38] J. Yu, et al., Lipid droplet remodeling and interaction with mitochondria in mouse brown adipose tissue during cold treatment, Biochim. Biophys. Acta 1853 (2015) 918–928, https://doi.org/10.1016/j.bbamcr.2015.01.020.
[39] J. Osuga, et al., Targeted disruption of hormone-sensitive lipase results in male sterility and adipocyte hypertrophy, but not in obesity, Proc. Natl. Acad. Sci. U.S.A. 97 (2000) 787–792, https://doi.org/10.1073/pnas.97.2.787.
[40] S. Wang, E.J. Dougherty, R.L. Danner, PPARγ signaling and emerging opportunities for improved therapeutics, Pharmacol. Res. 111 (2016) 76–85, https://doi.org/10.1016/j.phrs.2016.02.028.
[41] X.F. Yang, D.J. Shang, The role of peroxisome proliferator-activated receptor γ in lipid metabolism and inflammation in atherosclerosis, Cell Biol. Int. 47 (2023) 1469–1487, https://doi.org/10.1002/cbin.12065.
[42] N.G. Barra, B.D. Henriksbo, F.F. Anhe, J.D. Schertzer, The NLRP3 inflammasome regulates adipose tissue metabolism, Biochem. J. 477 (2020) 1089–1107, https://doi.org/10.1042/BCJ20190472.

[43] S. Pourdashti, et al., The size of human subcutaneous adipocytes, but not adiposity, is associated with inflammation, endoplasmic reticulum stress, and insulin resistance markers, Mol. Biol. Rep. 50 (2023) 5755–5765, https://doi.org/10.1007/s11033-023-08460-y.
[44] C. Muley, S. Kotschi, A. Bartelt, Role of ubiquilins for Brown adipocyte proteostasis and thermogenesis, Front. Endocrinol. 12 (2021), 739021, https://doi.org/10.3389/fendo.2021.739021.
[45] Z. Kocberber, N. Willemsen, A. Bartelt, The role of proteasome activators PA28alphabeta and PA200 in brown adipocyte differentiation and function, Front. Endocrinol. 14 (2023), 1176733, https://doi.org/10.3389/fendo.2023.1176733.
[46] J.H. Lee, et al., The role of adipose tissue mitochondria: regulation of mitochondrial function for the treatment of metabolic diseases, Int. J. Mol. Sci. 20 (2019), https://doi.org/10.3390/ijms20194924.
[47] G. Pidoux, et al., Optic atrophy 1 is an A-kinase anchoring protein on lipid droplets that mediates adrenergic control of lipolysis, EMBO J. 30 (2011) 4371–4386, https://doi.org/10.1038/emboj.2011.365.
[48] A.S. Rambold, S. Cohen, J. Lippincott-Schwartz, Fatty acid trafficking in starved cells: regulation by lipid droplet lipolysis, autophagy, and mitochondrial fusion dynamics, Dev. Cell 32 (2015) 678–692, https://doi.org/10.1016/j.devcel.2015.01.029.
[49] M. Boutant, et al., Mfn2 is critical for brown adipose tissue thermogenic function, EMBO J. 36 (2017) 1543–1558, https://doi.org/10.15252/embj.201694914.
[50] R. Schreiber, et al., Cold-induced thermogenesis depends on ATGL-mediated lipolysis in cardiac muscle, but not Brown adipose tissue, Cell Metabol. 26 (2017) 753–763 e757, https://doi.org/10.1016/j.cmet.2017.09.004.